Agricultural and Forest Meteorology 339 (2023) 109523

Contents lists available at ScienceDirect

Agricultural and Forest Meteorology

journal homepage: www.elsevier.com/locate/agrformet

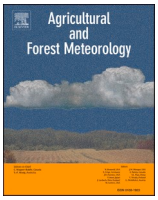

Two-level eddy covariance measurements reduce bias in land-atmosphere exchange estimates over a heterogeneous boreal forest landscape

Anne Klosterhalfen [a,*], Jinshu Chi [a,b], Natascha Kljun [c], Anders Lindroth [d], Hjalmar Laudon [a], Mats B. Nilsson [a], Matthias Peichl [a]

[a] Department of Forest Ecology and Management, Swedish University of Agricultural Sciences, Umeå, Sweden
[b] Earth, Ocean and Atmospheric Sciences Thrust, The Hong Kong University of Science and Technology (Guangzhou), Guangzhou, China
[c] Centre for Environmental and Climate Science, Lund University, Lund, Sweden
[d] Department of Physical Geography and Ecosystem Science, Lund University, Lund, Sweden

ARTICLE INFO

Keywords:
Tall tower eddy covariance
Heterogeneous landscape
Net ecosystem CO_2 exchange
Sensible heat flux
Latent heat flux
Footprint model FFP

ABSTRACT

Estimates of land-atmosphere exchanges of carbon, energy, water vapor, and other greenhouse gases based on the eddy covariance (EC) technique rely on the fundamental assumption that the flux footprint area is homogeneous. We investigated the impact of source area heterogeneity on flux estimates in single-level EC measurements over a managed boreal forest landscape. For this purpose, we compared single-level measurements with those from a two-level approach consisting of concurrent EC measurements at 60 and 85 m above the ground. This two-level set-up provided a unique opportunity to obtain nearly congruent diel footprint areas by combining data from the higher and lower levels during day- and nighttime, respectively.

We found that the variation in the averaged footprint area between day- and nighttime was reduced by up to 89% in the two-level approach compared to the single-level data at the higher level (85 m). Considering spring, summer, and fall months, the resulting relative potential bias in flux observations due to landscape heterogeneity was highest at short time steps ($\leq$ daily) ranging between 35% and 325% for half-hourly data. During winter months, when stable atmospheric regimes prevailed during day and night, the footprints within the diel course nearly overlapped also at a given single level and hence no improvement of flux estimates was found. The absolute cumulated sums for the study period (excluding winter months) of gross primary production, ecosystem respiration, latent heat, and sensible heat flux were underestimated by about 28%, 52%, 5%, and 3%, respectively, whereas that of net ecosystem CO_2 exchange was overestimated by about 109% in the single-level approach. Overall this study suggests that footprint heterogeneity may introduce considerable bias in single-level flux estimates — particularly at short time scales — with large implications for model-data fusion studies, site comparisons, and up- or downscaling of land-atmosphere exchange processes.

1. Introduction

Land-atmosphere exchanges of carbon, energy, water vapor, and other greenhouse gases are increasingly obtained with the eddy covariance (EC) technique. One fundamental assumption in this flux measurement method is that the surface of interest is flat and homogeneous over a large enough target area, so that the spatial representativeness is given for the measured fluxes (Giannico et al., 2018; Griebel et al., 2016; Rebmann et al., 2018; Schmid and Lloyd 1999). Still, the EC technique is also applied over complex and non-homogeneous terrain, which may introduce uncertainties in the measured fluxes. For heterogeneous surfaces, systematic errors are caused by increased occurrence of advection and non-closure of the energy balance, whereas random errors are introduced due to changes in the source area from which the measured fluxes originate (Giannico et al., 2018; Richardson et al., 2012). In regard to the latter, knowledge about the extent and position of the flux footprint and the distribution of scalar sinks and sources within the landscape that contribute to the vertical flux exchange becomes important (Barcza et al., 2009; Giannico et al., 2018; Griebel et al., 2016; Kim et al., 2018; Kljun et al., 2002; Rannik et al., 2012; Schmid and Lloyd 1999).

Various footprint models with their own advantages and restrictions

* Corresponding author.
E-mail address: anneklosterhalfen@gmail.com (A. Klosterhalfen).

https://doi.org/10.1016/j.agrformet.2023.109523
Received 3 June 2022; Received in revised form 28 April 2023; Accepted 17 May 2023
Available online 27 June 2023

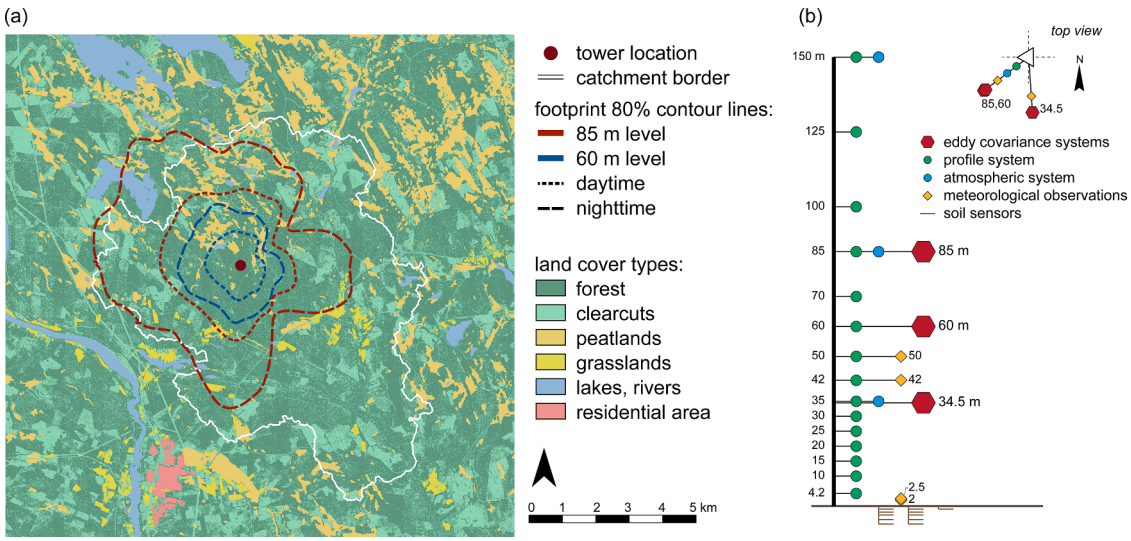

Fig. 1. (a) Location of the tall tower at Svartberget within the Krycklan catchment (white border) in northern Sweden, land cover types of the study area (Geografiska™ Sverigedata product), and footprint climatology (80% contour lines) of the entire study period for day- (dotted lines) and nighttime (dashed lines) and both eddy covariance systems. (b) Sketch of instrument set-up on the tall tower for the study time period. Numbers indicate measurement heights in meter.

have been developed to derive flux footprints for different time scales (Leclerc and Foken 2014; Schmid 2002; Vesala et al., 2008). The shape and extent of the flux footprint depend on wind direction, measurement height, surface roughness, and atmospheric stability. Thus, with increasing measurement height, for smooth surfaces, and/or more stable atmospheric conditions, the size of the footprint increases (Kljun et al., 2004; Rannik et al., 2012). Furthermore, because the wind direction and atmospheric stability usually vary at a sub-daily time scale, the footprint source area also varies within the diel course. Because stable regimes usually prevail at night and often change to unstable regimes during the day, footprint areas for a given tower site are often largest during nighttime. Moreover, the length of day and night can vary throughout the year depending on the latitude.

Due to the changing flux footprint area within the diel and seasonal course, the various sinks and sources are typically not equally represented in the observed fluxes of a heterogeneous landscape. Therefore, the aggregated flux time series could be biased due to the changing surface properties contributing to the net exchange (random error). Previous studies have estimated the magnitude of the total random error that included instrument and turbulence sampling errors next to the uncertainty introduced by footprint variability (e.g., Dragoni et al., 2007; Hollinger et al., 2004; Schmid et al., 2003). Oren et al. (2006) used multiple EC towers on ecosystem-level within a relatively homogeneous pine plantation to quantify the implications of spatial variability in ecosystem activity on turbulent fluxes. They described spatial variability on the basis of small heterogeneity in leaf area index and estimated the coefficient of spatial variation for flux data based on measurements from six EC towers with overlapping footprints. By combining the estimated coefficient of spatial variation with the observed annual net ecosystem CO_2 exchange (NEE) at one tower, they found that even in a homogeneous forest nearly half of the uncertainty in half-hourly flux data and annual NEE can be accounted to surface heterogeneity. Thus, the bias in flux measurements due to footprint variability over a heterogeneous surface could become even larger, but may differ between energy and carbon fluxes due to their specific dependencies on environmental and site characteristics (e.g., albedo, physiology, stomatal processes). Furthermore, by deriving relationships between physical drivers and fluxes for specific time periods and then applying these to other time periods (for instance for gap-filling), could include additional uncertainties due to differing sink and source areas depending on time of day, season, or intra-annual variability.

With EC instrumentations mounted to tall towers at higher heights, flux measurements can be obtained that are representative for the landscape/regional scale (i.e. tens of km^2, compared to the stand-level or ecosystem scale). One advantage of the larger footprint area is that it is more comparable to a large-scale model grid cell or the resolution of satellite data (e.g., Baker et al., 2003; Barcza et al., 2009; Chu et al., 2021; Desai et al., 2007; Keppel-Aleks et al., 2012; Sathyanadh et al., 2021). Also, the direct measurement of regional fluxes originating from a mixture of land cover types/ecosystems can be used to conduct and evaluate up- or downscaling procedures (e.g., Desai et al., 2008, 2015; Gelybó et al., 2013; Kim et al., 2006; Peltola et al., 2015; Soegaard et al., 2003; Wang et al., 2006; Xu et al., 2017; Zhang et al., 2014) and to improve our understanding of carbon dynamics, net biome production (Barcza et al., 2009; Chapin et al., 2006; Chi et al., 2020), and energy flux exchange (e.g., Butterworth et al., 2021). Especially, for a managed boreal forest landscape that consists of a mosaic of ecosystems including forests with different stand ages, clearcuts, peatlands, lakes, and streams, which all are coupled in a lateral direction and interact with each other, tall tower EC measurements provide a more direct estimate of the vertical flux exchange on the landscape scale (Chapin et al., 2006; Chi et al., 2019, 2020; Butterworth et al., 2021). However, since such tall tower flux measurements are usually conducted over heterogeneous terrain, these estimates are potentially biased by the variability in the flux footprint area within the diel course.

Conducting EC measurements on a tall tower, Davis et al. (2003) derived their best estimate for NEE of a heterogeneous mixed forest landscape in Wisconsin, USA, by combining EC flux data of three different measurement heights (30, 122, and 396 m; cf. Berger et al., 2001). Depending on atmospheric stability, boundary layer depth, and data availability, they chose measurements from a certain level for their final data set in order to, among other things, decrease the change in the footprint area. This dataset of optimized landscape NEE (sometimes extended by additional years after Davis et al., 2003) was used in various studies that focused on a wide range of different objectives and analysis of the land-atmosphere exchange of this mixed forest region (Baker et al., 2003; Desai 2010; Desai et al., 2008, 2015; Donnelly et al., 2019; Keppel-Aleks et al., 2012; Ricciuto et al., 2008; Schwartz et al., 2013; Wang et al., 2006). However, the degree of optimization of the NEE estimates was never explicitly stated to our knowledge. Overall, the approach of combining EC data from two or more measurement levels has rarely been applied within the flux community.

In this study, we combined flux measurements at two different levels on a tall tower to improve flux estimates for a heterogeneous boreal

forest landscape in northern Sweden. This two-level set-up provided the unique opportunity to select observations at the higher level (in 85 m) during daytime and at the lower level (in 60 m) during nighttime to obtain data with matching day- and nighttime footprint areas during the diel course and to quantify the bias induced by footprint differences. We chose day- and nighttime (using global radiation threshold of 10 W m^{-2}) as the criterion for the data combination because these time periods can be derived easily without any gaps from standard radiation measurements and are thus independent of EC measurements. Furthermore, this prevents frequent switching back and forth between different atmospheric stability classes and thus between measurement heights during the course of the day.

The aim of this study was to investigate how diverging day- and nighttime flux footprints affect EC flux estimates over heterogeneous terrain at various time scales. The main objectives were (1) to quantify the potential bias introduced by contrasting footprint characteristics during day- and nighttime by comparing NEE, latent heat flux (LE), and sensible heat flux (H) estimates from two-level and single-level measurements across various temporal scales, and (2) to analyze the implications of diel footprint divergence on data gap-filling and source partitioning.

2. Methods and materials

2.1. Site description

The study was carried out at the Integrated Carbon Observation System (ICOS, https://www.icos-sweden.se) Svartberget station (SE-Svb, 64° 15′ N, 19° 46′ E, 267 m a.s.l.), which is located within the Krycklan catchment (https://www.slu.se/krycklan) in northern Sweden (Fig. 1a). The study site is also part of the Swedish Infrastructure for Ecosystem Science (SITES, https://www.fieldsites.se/en-GB) network. The Krycklan catchment represents a typical managed boreal ecosystem including forest stands of different age, clearcuts, peatlands, grasslands, lakes, and streams (Chi et al., 2019, 2020; Laudon et al., 2013, 2021; Martínez-García et al., 2022). The forests are dominated by Scots pine, Norway spruce, and some birch including an understory dominated by ericaceous shrubs. The mean and maximum tree heights are about 23 m and 30 m, respectively, and the average leaf area index (LAI) at peak growing season about 2.97 ± 1.35 m^2 m^{-2}, but tree height and LAI estimates vary strongly within the catchment and stand age (Martínez-García et al., 2022). Forest management activities include clearcutting, thinning, drainage, and fertilization (Chi et al., 2020). The peatland areas are located predominantly in the northern parts of the catchment and are characterized as acid, oligotrophic, and minerogenic mires (Laudon et al., 2013, 2021). The climate conditions are cold temperate humid with an annual mean air temperature of 2.4 ± 0.8 °C and a mean annual precipitation sum of 638 ± 107 mm (1991-2020; https://www.slu.se/esf-referenceclimate).

2.2. Meteorological, ancillary environmental, and concentration profile measurements

In the framework of the ICOS data collection, meteorological measurements of air temperature (at 42 m measurement height), precipitation (2.5 m in a nearby open area), shortwave and longwave radiation components (50 m), photosynthetic photon flux density (50 m), air pressure (2 m), and relative humidity (42 m) are obtained on the tower at the study site (Fig. 1b). Furthermore, snow depth, soil temperature, soil water content, soil heat flux, tree temperature, and groundwater level are measured, each at multiple profiles and depths/heights. All these data were retrieved from the ICOS Carbon Portal (https://www.icos-cp.eu/, latest download July 2020, Peichl 2020a, 2020b, 2020c, 2020d).

Atmospheric greenhouse gas concentrations (CO_2 amongst others) are measured with the ICOS atmospheric system (G2401 gas concentration analyzer, Picarro, Inc., USA; sequential sampling scheme with 5-min measurement periods for each level) on the tall tower at 35, 85, and 150 m. Additionally, measurements of air temperature (105E temperature probe, Campbell Scientific, Inc., USA), CO_2, and H_2O concentrations (LI-7200 closed-path gas analyzer, LI-COR Biosciences, USA) are collected in a vertical profile system with measurement levels at 4.2, 10, 15, 20, 25, 30, 35, 42, 50, 60, 70, 85, 100, 125, and 150 m. The air temperature is measured continuously for each level separately (5-min frequency). The gas concentrations are measured with a sequential scheme with one gas analyzer, where the measurement height is switched every 30 s and, thus, each of the fifteen levels is repeatedly measured every 7.5 min. More detailed description of the meteorological and ancillary instrumentation at Svartberget can be found in Chi et al. (2019).

2.2.1. Quality check and control of ancillary measurements

All meteorological and environmental measurements were checked with thresholds set for the local conditions. Additionally, measurements of the ICOS atmospheric system and the vertical profiles were discarded when they were obtained during maintenance work on the instruments or the tower structure, and were filtered for spikes. These spikes were detected by applying limits determined with the mean ± 3x standard deviation of the concentration data for a time window of 10 days.

2.2.2. Gap-filling of ancillary measurements

The meteorological and environmental measurements were gap-filled in multiple steps. First, small gaps (≤ 2 h) were filled via linear interpolation. Second, all remaining gaps were filled by using a linear relationship (reduced major axis regression after Webster 1997) between neighboring sensors (e.g., sensors in different measurement heights), between two different variables or instruments (e.g., air and canopy temperature, concentration measurements of profile and atmospheric system), and/or between two nearby sites (e.g., for all meteorological data between SE-Svb and back-up meteorological stations with a maximum distance of 14 km). Third, all remaining gaps ≤ 36 h were filled with the mean diurnal course of a 10-days window of the variable. Last, all remaining gaps were filled with the rolling mean of a 14-days window of the variable.

2.3. Tall tower eddy covariance flux measurements

In total, three EC systems were installed on the 150 m tall tower in Svartberget, measuring CO_2, water vapor, and energy flux exchange between the boreal landscape and atmosphere. The ICOS ecosystem-level EC system is mounted at 34.5 m (here, we only use its data for quality check, cf. Appendix C, and footprint modeling, cf. Section 2.5). This study focused on two additional EC systems: (1) EC system consisting of a CSAT3 3-D sonic anemometer and an EC155 closed-path gas analyzer (Campbell Scientific, Inc., USA) at 60 m measurement height, and (2) EC system consisting of an ultrasonic anemometer uSonic-3 Omni (METEK Meteorologische Messtechnik GmbH, Germany) and a FGGA-24EP closed-path greenhouse gas analyzer (LGR, Los Gatos Research, Inc., USA) at 85 m. The FGGA is located on the ground-level and connected with an about 100 m long Synflex 1300 tubing with an outside diameter of 12 mm (cf. Chi et al., 2020). The air sampling flow rate was about 40 L min^{-1}. Both EC systems sample at a 10 Hz frequency. The study time period was from 1st September 2018 until 15th July 2019 (15,264 half-hourly time steps) starting at the installation date of the 85 m-level EC system in the beginning of September 2018 and ending due to an instrument malfunction of the 60 m-level EC system starting mid-July 2019.

2.3.1. Flux raw data processing

The raw data of the two tall tower EC systems were processed with the EddyPro® Software (v7.0.9, LI-COR Biosciences, USA) to obtain half-hourly CO_2 and energy fluxes. We followed mainly the ICOS

protocol after Sabbatini et al. (2018) with the following adjustments. For the raw data quality check, the allowance of missing samples in one half-hour was increased from 10% to 20%, and the absolute limits of sonic temperature were adjusted to the local plausible range and to the operating temperature range of the gas analyzers (-30 °C to +40 °C). Sonic temperature raw data obtained with the METEK sonic anemometer in 85 m was crosswind-corrected (METEK GmbH 2012) before the flux processing with EddyPro®, because the correction is not implemented in the anemometer's firmware and the anemometer type was not implemented in the EddyPro® version. The double rotation method was used for the anemometer tilt correction (Rebmann et al., 2012). To correct for the time lag between gas analyzers and anemometers, the compensation was done by the time lag optimization approach (Sabbatini et al., 2018). Due to the long tubing of the 85 m-level EC system, the medians of its time lags were 23.9 s and between 23.0 and 29.3 s (depending on relative humidity) for CO_2 and water vapor, respectively. For the high-frequency spectral correction, the approach after Ibrom et al. (2007) was applied. As we used the given high-frequency mixing ratios from the gas analyzers as input for our flux data processing, a correction for density fluctuations was not necessary, except for the water vapor concentration of the 85 m-level EC system, where we applied the WPL-correction as it is implemented in EddyPro®.

Due to the differing instrumental set-up, we conducted an instrument comparison of the gas analyzers and sonic anemometers of both EC systems (Appendix B). For a comparison of wind roses see Fig. S2 in the supplementary material. Unfortunately, it was not logistically possible to install both EC systems next to each other at the same height for a short time period, which would have been optimal. Thus, we compared measurements of both EC systems which were obtained under similar and optimal conditions and of (presumably) similar flux footprints (Fig. B1 in Appendix B). Furthermore, we aligned the concentration measurements of both gas analyzers in reference to the measurements of the vertical profile. By comparing half-hourly CO_2 and H_2O measurements between the profile system (reference) and each EC system, the absolute offsets and regression slopes were obtained during similar and optimal conditions (see description in Appendix B) — to ensure relative similar source areas. Then, the CO_2 and H_2O raw data (10 Hz data) of each EC system was corrected based on the estimated offsets and slopes, and fluxes were reprocessed with EddyPro®. Thus, in the following study, flux estimates of NEE, LE, and H were obtained based on the aligned concentration raw data.

During winter, the sonic anemometers were heated occasionally to prevent ice or snow on the instruments, but here data points obtained during heating were not discarded before flux calculation (see Appendix C).

2.3.2. Storage term correction of flux data

The half-hourly fluxes of CO_2, LE, and H were corrected with their storage terms following the ICOS protocol after Montagnani et al. (2018). The storage terms between soil surface and EC systems were estimated based on air pressure and the vertical temperature and concentration profile measurements, which were obtained between the respective EC measurement height and the lowest profile measurement level at 4.2 m, where the latter measurements also represented the concentration of the bottom layer between soil surface and 4.2 m. The profile data was quality-checked, gap-filled (see Section 2.2), and then aggregated to 15-min time steps. Storage terms were excluded if they were outside a reasonable range (Table A1 in appendix). Before adding these filtered storage terms to the flux observations, they were aggregated to half-hourly time steps. In the following discourse the fluxes NEE, LE, and H always include the storage terms.

2.3.3. Quality check and control of flux data

To ensure a high quality of the processed, half-hourly fluxes, a further quality control was carried out as previously described in detail by Chi et al. (2019) for the same site. In brief, data were discarded when quality criteria were not met and following conditions applied: data received bad quality flag in the raw data processing (flag 2 for the "0–1–2 system" after Mauder and Foken 2004), was outside absolute limits (Table A1), was influenced by wind distortion due to the tower structure, was obtained during instrument maintenance, the anemometer or gas analyzer uptime was low, or the power had failed.

Flux time series were also filtered for periods without adequate atmospheric boundary layer mixing. Wharton et al. (2009) introduced turbulence intensity parameters (I_w and I_u), looking at the ratio of mean unrotated vertical (w) or horizontal rotated wind velocity (u) and a modified turbulent velocity scale (u_{TKE}, which is dependent on turbulent kinetic energy) to detect time periods with prevailing vertical or horizontal advection fluxes, respectively. The threshold $I_{w,crit}$ was determined with the mean ± 1x standard deviation of the time series of the turbulence intensity ratio I_w, and the threshold $I_{u,crit}$ was determined with the mean + 1x standard deviation of I_u. $I_{w,crit}$ and $I_{u,crit}$ were ±0.186 and 5.3 for the 60 m-level EC system and ±0.295 and 7.3 for the 85 m-level EC system, respectively. When positive ratios were larger or negative ratios lower than the determined thresholds, flux data were excluded. Also, time periods with a lower boundary layer height (h_{bl}) than the highest EC measurement level (≤ 85 m) were discarded. Estimates of h_{bl} were taken from the ERA5 hourly data (fifth generation ECMWF atmospheric reanalysis) of the corresponding grid cell of our study site for 2018 and 2019 (Hersbach et al., 2018). These data were resampled to half-hourly data by linear interpolation, and then smoothed by taking the mean over a moving window of 12 h to decrease uncertainties.

Furthermore, NEE and LE were discarded when spikes occurred in the CO_2 and H_2O mixing ratios. These spikes were detected by applying limits determined with the mean ± 3x standard deviation of the concentration data for a time window of 10 days. Also, outliers in NEE, LE, and H flux data were detected directly with the mean absolute deviation approach with the threshold value 5 for NEE and 7 for LE and H (Papale et al., 2006; note that these threshold values are designated as z in Papale et al., 2006).

After flux data raw processing, about 10% for the 85 m-level EC system of the half-hourly flux data (NEE, LE, or H) were missing, only up to 5% were discarded due to a too low h_{bl}, up to 15% were discarded due to filtering for advection, and in total after the complete quality-check (incl. filtering for maintenance time, wind distortion etc.) up to 46-56% of flux data were removed. For the 60 m-level EC system, relative fractions of missing and removed flux data were 16% after flux processing, up to 4% due to a too low h_{bl}, up to 11% due to advection, and up to 44-51% after the completed quality check (cf. Table A2 in appendix, Fig. S3 in supplementary material).

2.3.4. Gap-filling and source partitioning of flux data

In this study, fluxes from the ecosystem to the atmosphere (upward) are defined as positive fluxes, and downward fluxes as negative. NEE, LE, and H flux data were gap-filled using the R-package REddyProc (v3.6.3, Wutzler et al., 2018). This flux post-processing tool applies the marginal distribution sampling strategy that combines a look-up table and a mean diurnal course approach for gap-filling. The necessary meteorological data (air temperature and vapor pressure deficit) were taken from the vertical profile measurements at the respective EC measurement height. The gap-filled NEE was partitioned into the two flux components gross primary production (GPP) and total ecosystem respiration (R_{eco}; NEE = GPP + R_{eco}), using the nighttime flux partitioning approach after Reichstein et al. (2005) (using the relationship between NEE nighttime fluxes to air temperature), which is also implemented in the REddyProc package.

2.4. Combination of the two-level eddy covariance measurements

In this study, we combined flux measurements of the higher level (85 m) EC system during daytime and the lower level (60 m) during

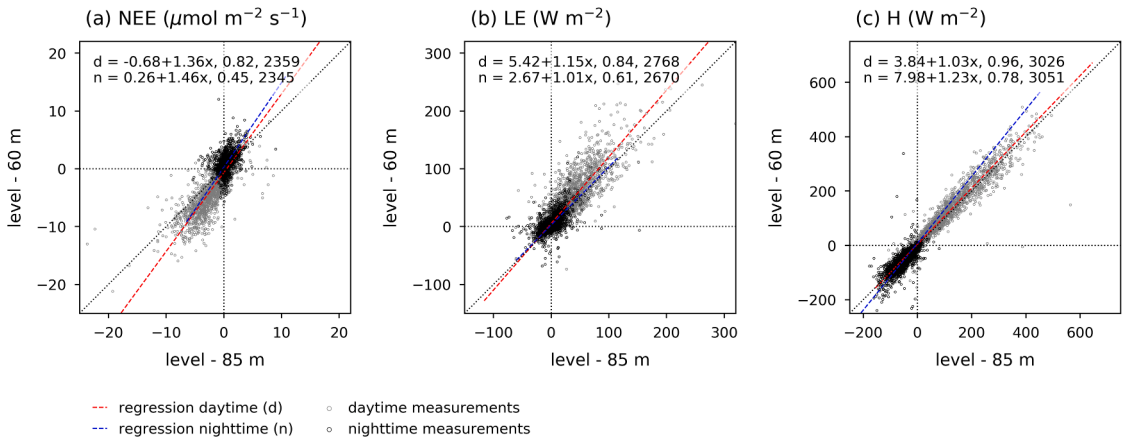

Fig. 2. Comparison of half-hourly, quality-checked and storage term corrected day- (gray circles) and nighttime (black circles) measurements of both eddy covariance systems (85 m versus 60 m measurement height) for (a) net ecosystem exchange (NEE), (b) latent heat (LE), and (c) sensible heat (H) flux during the study time period from September 2018 until July 2019. Equations of each reduced major axis regression (d: daytime, n: nighttime), correlation coefficient and sample size are listed in this order.

nighttime to acquire data obtained from a more similar footprint area during the diel course. For this two-level data, the quality-checked and storage term corrected measurements were chosen. The gap-filling and source partitioning methods were then applied to these combined two-level data in the subsequent step as described in Section 2.3.4.

We distinguished between day- and nighttime on the basis of a threshold for global radiation < 10 W m^{-2} following Wutzler et al. (2018). Time periods with very low radiation due to cloudiness and precipitation were correctly associated to night- or daytime by estimations of sunrise and sunset times (by means of latitude, longitude, and local time). The considered study period of 10.5 months comprised 15, 264 half-hours consisting of 6571 daytime (43%) and 8693 nighttime (57%) half-hours.

2.5. Footprint analysis

For the description of the day- and nighttime flux footprint areas of the two EC systems, the two-dimensional parameterization for footprint predictions FFP after Kljun et al. (2015) was applied to quality-checked, half-hourly turbulence data (filtered for outliers, advection, too low h_{bl}, and wind distortion). FFP was selected as it is based on the Lagrangian stochastic Particle Footprint model of Kljun et al. (2002) and is one of the very few footprint models that is valid for measurements at tall towers, where sensors are often above the surface layer. It is also valid for convective to stable atmospheric stability conditions (see Kljun et al., 2015). Next to variables easily obtained with the EC technique, the displacement height (d), roughness length (z_0), and h_{bl} are needed as input parameters for this footprint model. To account for the heterogeneity of the boreal landscape, d and z_0 were estimated for each 30° wind sector, using the turbulence measurements of the 60 m-level EC system and the ICOS EC system at 34.5 m (see Chi et al., 2019 and Appendix D for a detailed description). As for the flux quality check (Section 2.3.3), estimates of h_{bl} were taken from the ERA5 hourly data (fifth generation ECMWF atmospheric reanalysis) of the corresponding grid cell of our study site for 2018 and 2019 (Hersbach et al., 2018). These data were resampled to half-hourly data by linear interpolation.

The flux footprint indicates the smallest possible source area, from which a given relative fraction of the observed flux originates, and is derived for each half-hourly data point. For longer time series the so-called footprint climatology can be derived as an aggregation of all (half-)hourly flux footprints for a selected time period (Kljun et al., 2015). Here, the footprint climatology was derived for a) the entire study period from September 2018 until July 2019, b) each season, and c) each month of the study period for day- or nighttime individually. We defined the different seasons within our study period depending on meteorological conditions and day length. Thus, our usage of the terms 'winter', 'summer', and 'transition' months ('fall': September-October 2018; 'spring': March-April 2019) was based on the magnitudes of net radiation, air temperature, and vapor pressure deficit, and was independent of, for instance, phenology or ecology (Fig. S1 in supplementary material).

Additionally, the sensitivity of the estimated footprint area was tested regarding the input h_{bl}. In this sensitivity analysis, h_{bl} was changed by ±5% or ±10%, respectively, and the seasonal footprint climatology was derived for each.

The geospatial data of the land cover types were taken from Chi et al. (2019) (Geografiska™ Sverigedata product). The footprint simulations and geospatial data had the same spatial resolution of 10×10 m^2.

2.6. Bias calculation

In this study, we chose relative differences to compare the various data sets (single- or two-level), and to quantify the bias in flux measurements obtained with a changing footprint area. Estimating the difference related to an absolute mean flux, makes the bias independent of the absolute flux magnitudes and related error magnitudes, both of which differ between seasons. With the two-level combination, we expect the bias to be reduced due to better matching day- and nighttime footprints and thus flux estimates should be improved. Based on these judgments, we define the two-level data set in the following analysis as reference. The relative differences (Δflux in %) were quantified as the difference between the single-level ($flux_{85}$) and the two-level reference ($flux_{ref}$) data in relation to the absolute mean flux in different time steps:

$$\Delta flux_{i,t} = \frac{flux_{85_{i,t}} - flux_{ref_{i,t}}}{\left| \frac{1}{n} \sum_{i=0}^{n} flux_{ref_{i,t}} \right|} \cdot 100 \quad (1)$$

where i indicates the data's time step (e.g., half-hourly, hourly, daily, etc.), n the number of data points for which $flux_{85}$ and $flux_{ref}$ data were available, and t the chosen corresponding time window (for each season or entire study period). Here, also winter months were always excluded (cf. Sections 3.2, 3.3). Moreover, for $\Delta flux_{i,t}$ in half-hourly data, the direct measurements of the 85 m-level EC system during daytime were also excluded because these data points matched between both data sets. Positive $\Delta flux_{i,t}$ indicates an overestimation of the fluxes by the single-level measurements (but note: for GPP, which is here defined to be $<$ 0, a positive $\Delta flux_{i,t}$ indicates an underestimation of CO_2 uptake and more positive numbers), and a negative $\Delta flux_{i,t}$ an underestimation of

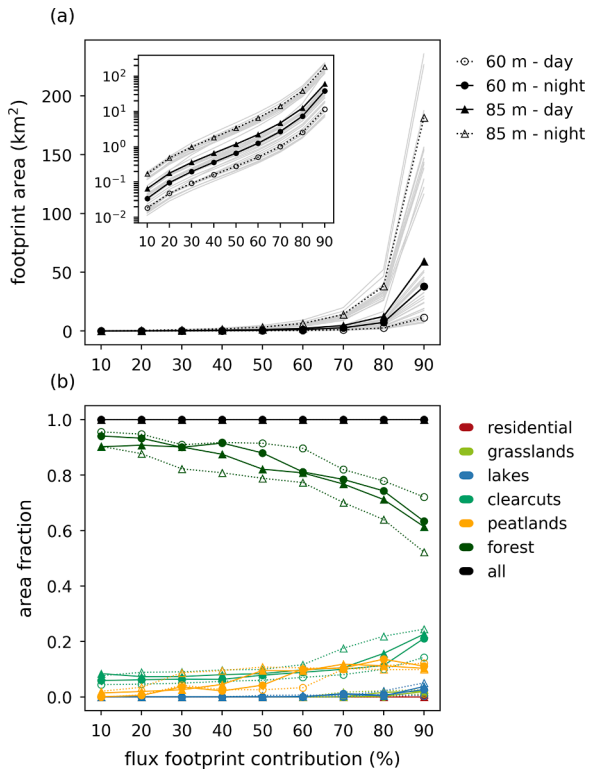

Fig. 3. (a) Footprint area and (b) fraction of area for each land cover type depending on relative flux contribution of the study period's footprint climatology for day- and nighttime. Gray lines in the upper panel represent the areas depending on the relative flux contribution of the monthly footprint climatology for day- and nighttime. The inset graph in the upper panel shows the footprint area in a logarithmic scale. In both panels, solid lines depict the data linked to and/or used for the two-level combination.

the fluxes.

Following Eq. (1), the mean absolute difference between single- and two-level data was calculated in relation to the absolute mean flux of the entire study period in the different time steps:

$$\mathrm{PBias} = \frac{\frac{1}{n}\sum_{i=0}^{n}\left|\mathrm{flux}_{85_i} - \mathrm{flux}_{\mathrm{ref}_i}\right|}{\left|\frac{1}{n}\sum_{i=0}^{n}\mathrm{flux}_{\mathrm{ref}_i}\right|} \cdot 100 \quad (2)$$

This relative potential bias PBias represents the worst-case scenario, because the bias adds up for each flux and for the different time steps. Again, winter months were excluded, as well as, for PBias in half-hourly data, the direct measurements of the 85 m-level EC system during daytime were excluded.

3. Results

In the following subsections, we first analyzed the directly measured, quality-checked EC data of both measurement levels regarding their magnitudes (Section 3.1). Second, we applied the footprint model to day- and nighttime data of both EC systems, and compared the footprint areas and the contributions of the different land cover types between both measurement levels (Section 3.2), in order to check how well the day- and nighttime footprints matched for the two-level data (combination of daytime 85 m- and nighttime 60 m-level measurements). In Section 3.3, the final gap-filled and source partitioned flux data were compared between the single- and two-level data sets across multiple time scales.

3.1. Tall tower eddy covariance flux measurements

As expected, the half-hourly daytime NEE fluxes were mostly negative (net CO_2 uptake by the ecosystem), and daytime LE and H were mostly positive (net energy release) at both EC measurement heights (Fig. 2). During nighttime, net CO_2 release prevailed with positive NEE, LE was mostly positive and close to zero, and H was usually negative. According to the regressions' slopes (> 1.00) of the comparison between both measurement levels, the absolute magnitudes of the 60 m-level EC measurements were usually larger than those of the 85 m-level. The regression slopes for the nighttime NEE and H data were ≥ 1.23, such that at the lower measurement level more positive (higher) NEE fluxes and more negative (lower) H fluxes were measured than at the higher measurement level. By combining the data of both levels, i.e. by replacing the nighttime data in the time series of the 85 m-level EC system with measurements of the 60 m-level, the amplitudes in NEE and H increased in comparison to the original fluxes measured at 85 m (Fig. 2). Because R_{eco} is estimated based on the nighttime NEE fluxes, its

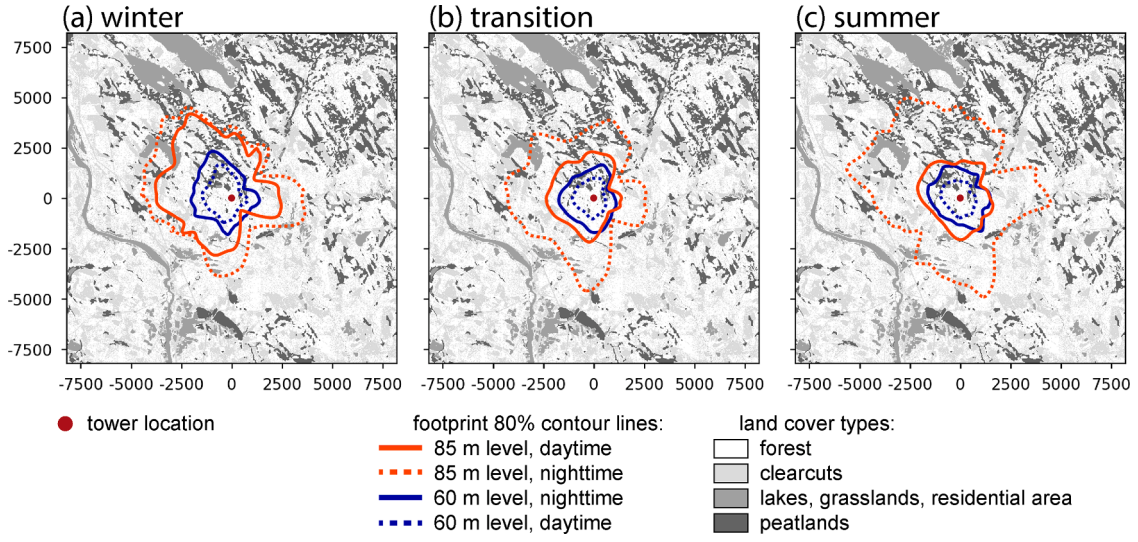

Fig. 4. (a) Footprint climatology for both eddy covariance systems for each season: (a) winter (Nov-Feb), (b) transition months (Sep-Oct, Mar-Apr), and (c) summer (May-mid Jul). The 80% contour lines are shown for day- and nighttime individually. Numbers on x- and y-axes indicate the distance from the tower in meters.

Table 1
Aggregated footprint areas in km^2 (80% flux footprint contribution) for both eddy covariance systems, for day- and nighttime individually, and for each season and the entire study period. The ratio of nighttime over daytime footprint areas (italic) shows how much larger the footprint area was during nighttime than during daytime for each measurement level, and for the two-level data set (last column; daytime 85 m- and nighttime 60 m-level).

	85 m-level			60 m-level			Two-level
	Day (km^2)	Night (km^2)	*Ratio (-)*	Day (km^2)	Night (km^2)	*Ratio (-)*	*Ratio (-)*
Winter	25.0	38.2	*1.53*	3.7	8.0	*2.17*	*0.32*
Transition months	10.6	34.1	*3.21*	2.3	6.2	*2.67*	*0.59*
Summer	10.0	51.8	*5.19*	2.3	6.6	*2.86*	*0.66*
Entire period	12.4	38.0	*3.07*	2.6	7.3	*2.86*	*0.59*

magnitude will also be larger for the two-level data during night- and also daytime, and have an impact on GPP estimates. The time series of the half-hourly observations for both EC measurement heights are shown in Figure S3 in the supplementary material.

3.2. Comparison of footprint areas between both measurement levels

The footprint climatologies of both EC systems for the entire study period are shown in Fig. 1a with the 80% flux contribution contour lines (red for 85 m- and blue for 60 m-level EC system), where a distinction is made between the footprint climatology of day- or nighttime data. Because of the higher measurement height, the footprint areas extended further for the 85 m-level EC system than for the 60 m-level. Fig. 1a already indicates that when combining data of the two measurement heights we obtain data measured of a less variable source area in the diel course (dotted red and dashed blue contour line). Naturally, with increasing flux footprint contribution the area increased (Fig. 3), where the 90% flux contribution areas became in all cases relatively large and varied a lot between months as indicated by the gray lines in Fig. 3a. The area fraction of forest decreased with increasing footprint contribution and footprint extent, while the area fraction of clearcuts and peatlands mostly increased (Fig. 3b). The fractions of grasslands, lakes, rivers, and residential areas were small and did not differ much between footprint extents.

The difference in area between the daytime 85 m- and nighttime 60 m-level footprint was on average much smaller than between day- and nighttime for each single measurement level (Fig. 3a). Furthermore, the area fractions of each land cover type matched very well between day- and nighttime for the two-level data, better than for each EC system on its own. An exception was observed for the area fraction of forest and peatlands, where a larger area of peatlands fell within the 40%- and 50%-footprint contour line of the 85 m-level EC system, but was not 'seen' by the 60 m-level EC system, due to its smaller footprints.

However, the footprint climatologies for each season indicated differences in day- and nighttime footprint proportions between seasons (Fig. 4, Table 1, cf. Fig. S4 in supplementary material with footprint climatologies for each month). In summer (May-mid July, Fig. 4c) and transition months (September-October, March-April, Fig. 4b) the seasonal averaged footprint areas of the two-level data set matched relatively well with a small difference in footprint area size below 4.4 km^2. The difference between day- and nighttime footprints for the 60 m-level EC system was similar in size, but much larger with up to 42 km^2 for the 85 m-level (Table 1). The nighttime footprints were up to 5 times larger than the daytime footprints for the 85 m-level. For the two-level combination, the nighttime footprints were about a two fifth (34-41%) smaller than the daytime footprints (Table 1). This confirms the above described results as seen in Fig. 3. However, in winter months (November-February, Fig. 4a) the daytime footprint areas of both EC systems were larger due to an increase in stable stratification cases and, thus, of a more similar size as the respective nighttime footprint area. For each single level, nighttime footprints were about two times larger than daytime footprints, and for the two-level combination, nighttime footprints were up to three times smaller than daytime footprints. Hence, the two-level combination did not decrease the footprint variability significantly during winter months (Table 1).

The estimated seasonal footprint climatologies were sensitive only to a small extent towards the estimate of h_{bl} (Table 2), where footprint areas changed by up to 4.4% due to a change in h_{bl} by 5% or 10%. Considering the largest estimated footprint area of about 52 km^2 for the 85 m-level EC system during nighttime for summer, an 5% increased h_{bl} estimate would result in a by 2.3 km^2 larger footprint area. In general, an increase in h_{bl} yielded in a decrease in footprint area, and vice versa, with a few exceptions. The relative change in footprint areas of the 85 m-level EC system were usually slightly larger than of the 60 m-level. However, a clear dependency of the change in footprint area on season or day- and nighttime could not be observed.

Stable atmospheric conditions prevailed during nighttime in all seasons and during daytime in winter, as can be seen in the diel courses of the atmospheric stability regime (Fig. 5, top panels). During stable conditions the half-hourly footprint areas were about 3-5 km^2 for the 85 m-level EC system and about 1-2 km^2 for the 60 m-level, and they decreased with neutral or convective conditions (Fig. 5, middle panels). Accordingly, the footprint area fraction of forests decreased with increasing footprint area (Fig. 5, bottom panels). During winter months, there was no correlation between incoming radiation (day- or nighttime) and stability regime, and with that the diel dynamic in the footprint variability disappeared. So, the reduction or improvement of the footprint variability by the two-level combination was dependent on seasons. However, in general the orientation and dimension of the flux footprint was highly variable throughout the study period.

To summarize, by selecting the lower measurement level during nighttime, the corresponding footprint area of nighttime flux observations decreased compared to the 85 m-level footprint area, and the footprint area fraction of forest increased and that of clearcuts and peatlands decreased. With this two-level combination the averaged footprint during nighttime was smaller than during daytime, but the footprint variability within the diel course was decreased by up to 89% (Table 1; ratio between differences in footprint area of the two- and 85 m-level). This good agreement of day- and nighttime flux footprints depended on dynamics in the atmospheric stability regime at a monthly or seasonal scale.

Table 2
Relative changes (in %) in estimated footprint areas (80% flux footprint contribution) due to changes in the boundary layer height (h_{bl}) by ±5% and ±10% for both eddy covariance systems, for day- and nighttime individually, and for each season.

		85 m-level				60 m-level			
Change in h_{bl} by		-10%	-5%	+5%	+10%	-10%	-5%	+5%	+10%
Winter	Day	4.4	1.6	-1.5	-0.8	2.1	0.8	-1.4	-1.6
	Night	2.8	-1.4	-2.0	0.2	0.7	0.6	0.6	-1.5
Transition	Day	1.7	0.8	-1.7	-1.1	0.5	0.8	-0.7	-1.5
	Night	4.2	3.7	-0.5	-1.0	0.6	1.5	-0.1	-0.2
Summer	Day	1.9	1.2	-1.4	-2.6	1.4	0.7	-0.6	-1.2
	Night	2.0	4.4	-0.1	-3.9	3.0	2.8	0.6	0.2

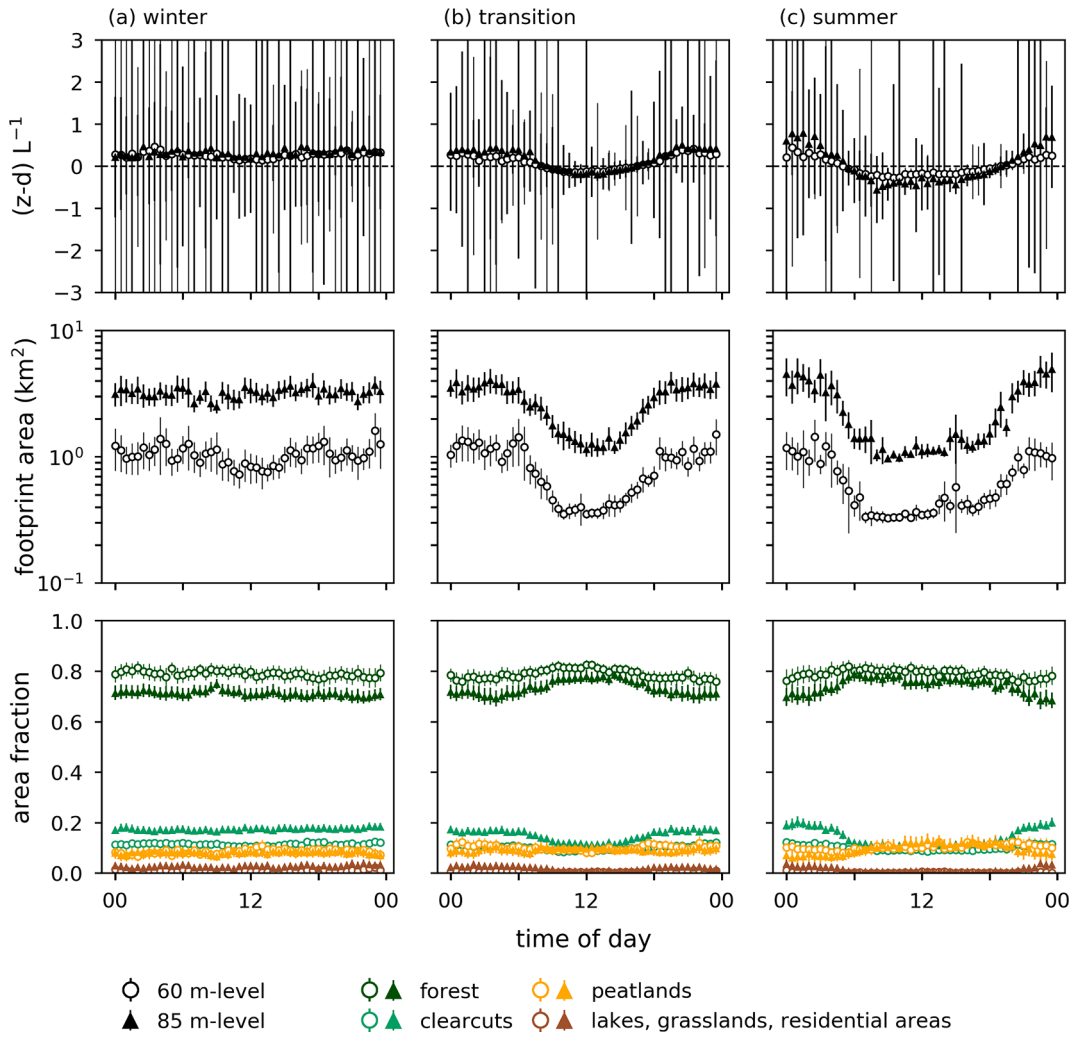

Fig. 5. Median diel course (local time) of atmospheric stability depicted as (z-d)/L (top panels), footprint area (middle panels), and area fraction for each land cover type (bottom panels) for both single-level measurements, individually depicted for (a) winter (Nov-Feb), (b) transition months (Sep-Oct, Mar-Apr), and (c) summer (May-mid Jul). The footprint areas and area fractions are shown for the 80% flux contribution. Error bars indicate the 95% confidence intervals of the mean values.

3.3. Comparison of single- and two-level flux data

In the following comparison between the single- and two-level data sets, we excluded the winter months November 2018 until February 2019, as the footprint analysis had shown that the variability of the day- and nighttime footprints was similar or increased with the combination of the two measurement levels for these months. This indicates that the flux estimates for the two-level data set were (even more) biased due to changes in the footprint in the diel course. For the remaining months, September-October 2018 and March-July 2019, the bias should be reduced due to better matching day- and nighttime footprints and, thus, flux estimates have been improved. Based on these judgments, we define the two-level data set in the following analysis as reference ($flux_{ref}$). With the comparison between this reference and the single-level data set of the 85 m-level EC system ($flux_{85}$) or the 60 m-level ($flux_{60}$, see supplementary material Fig. S7-S10), we could now estimate the bias in flux data obtained by only one measurement height.

Even though incoming radiation, air temperature, vapor pressure deficit, and day lengths were similar during transition months (Fig. S1 in supplementary material), flux magnitudes were very small during spring (March-April 2019) in comparison to fall (September-October 2018), mainly due to the snow cover (Figs. S3, S5, S6 in supplementary material). Thus, in the following we only show relative differences ($\Delta flux_{i,t}$ in %) between the single-level ($flux_{85}$) and two-level reference ($flux_{ref}$) data in relation to the absolute mean flux in different time steps, which are independent of the flux magnitude (Eq. (1)). For Fig. 6, $\Delta flux_{i,t}$ was calculated by choosing the absolute mean daily flux for each season (i = daily; t = spring, summer, or fall months) as a denominator, and for Fig. 7 by choosing the absolute mean flux of the entire study period for different time steps (i = half-hourly, hourly, daily, weekly, monthly, per season, entire study period; t = entire study period).

The relative daily differences between single- and two-level data for NEE (ΔNEE) was mostly negative during fall (Fig. 6). During spring and summer ΔNEE was almost compensated in the course of the season. ΔR_{eco} was mostly negative during all seasons and ΔGPP was mirrored to ΔR_{eco}. Therefore, the magnitudes of CO_2 release and uptake were both underestimated at the single-level. However, these underestimations of the opposing fluxes affected the NEE differently between seasons: smaller/more negative net exchange during fall, high variable net exchange during spring, and only a small difference during summer. ΔLE was mostly negative, so the magnitude of LE was mostly underestimated at the single-level. The magnitude of H was mostly overestimated in spring, and was mostly underestimated in fall and summer. Note, that these relative biases are related to each seasonal average flux magnitude. The cumulated curves in Fig. 6 represent the effect of using only one level compared to two levels on the cumulated sums per season. Following the cumulated curves, the relative bias in all carbon and energy flux estimates was highest during fall.

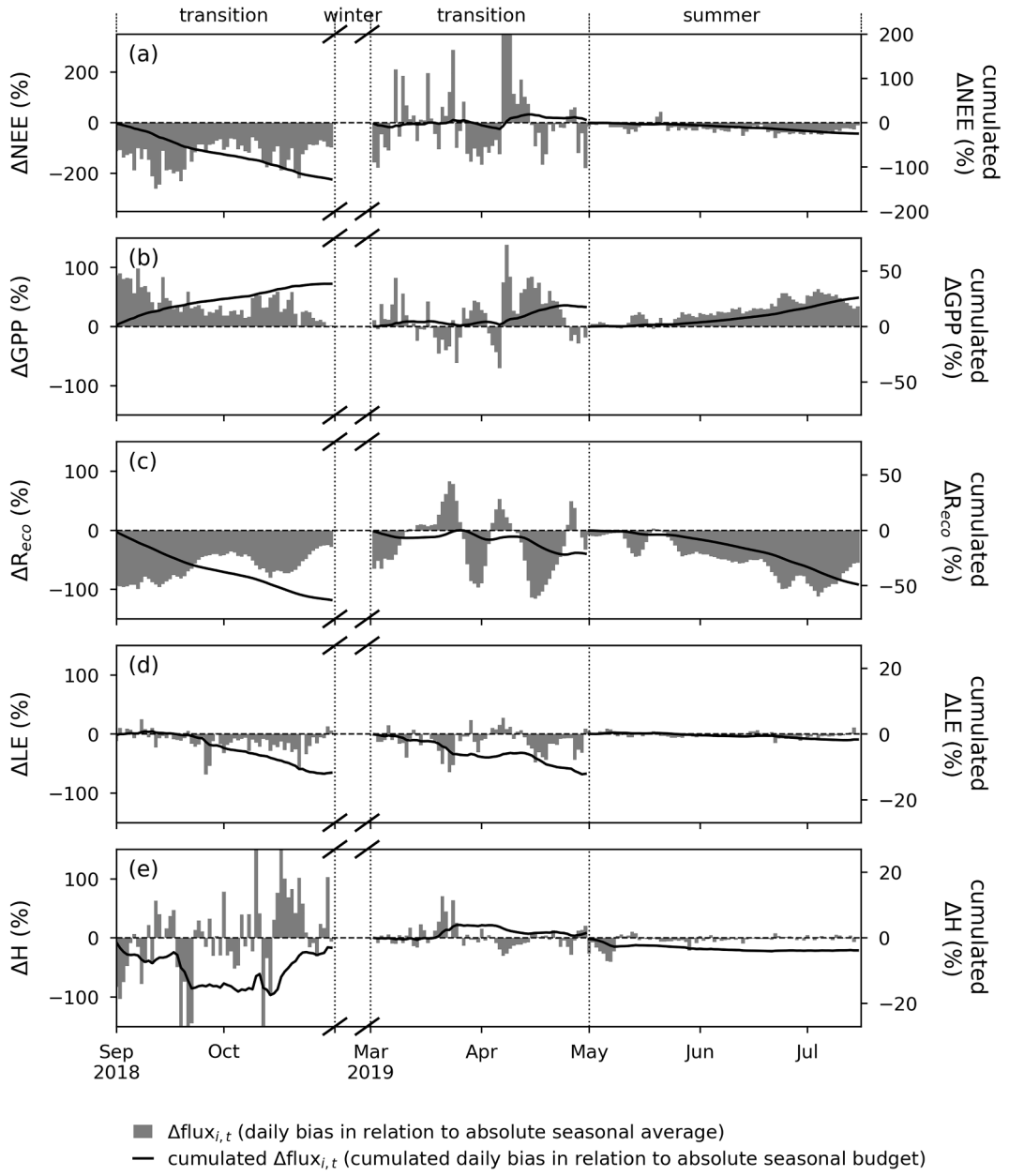

Fig. 6. Relative differences ($\Delta flux_{i,t}$ in %, cf. Eq. (1)) between 85 m- and two-level data in relation to the absolute daily mean flux of each corresponding season in the daily (a) net ecosystem exchange (NEE), (b) gross primary production (GPP), (c) ecosystem respiration (R_{eco}), (d) latent heat (LE), and (e) sensible heat (H) flux estimates (subscripts i = daily, t = each season). $\Delta flux_{i,t}$ is shown for each variable per day (left y-axis, gray bars) and cumulated over each season (right y-axis, black line).

Considering the cumulated sums for the entire study period (excluding the winter months), the absolute differences between the 85 m- and two-level sums were smaller than the absolute differences between the 60 m- and two-level sums, except for R_{eco} (Table 3). Cumulated R_{eco} was almost identical between the 60 m- and two-level data, because the nighttime flux-based source partitioning approach after Reichstein et al. (2005) was used. Comparing the 85 m- and two-level data, the sums changed by 109%, -28%, -52%, -5%, and -3% for NEE, GPP, R_{eco}, LE, and H by measuring only on one level.

The relative differences ($\Delta flux_{i,t}$) between single- and two-level data for different time steps in relation to the absolute mean flux of the entire study period are shown in Fig. 7. For the carbon and energy fluxes, the range and standard deviations of $\Delta flux_{i,t}$ decreased significantly from half-hourly to seasonal time steps. However, mean $\Delta flux_{i,t}$ differed not much between the different time steps. For the energy fluxes mean $\Delta flux_{i,t}$ was always relatively small, because under- and overestimation of fluxes could cancel each other out. But if a smaller time window of half-hourly, hourly or daily data would be chosen, then the chance of flux under- or overestimation increases. The reason for large $\Delta flux_{i,t}$ in (half-)hourly data was certainly mostly the difference between footprint extensions of the two different measurement heights, because in this time step no data was really combined and aggregated, yet. Still, by choosing data from the lower level during night, the extent of footprints should be more similar to the extent of footprints during daytime (data from upper level), even though the direction and wind speed could still differ within the diel course, but usually not between measurement levels (Fig. S2 in supplementary material). The variance of $\Delta flux_{i,t}$ was usually larger during transition months than during summer (not shown). Obviously, relative differences between the single- and two-level data were the largest during nighttime, because here the data

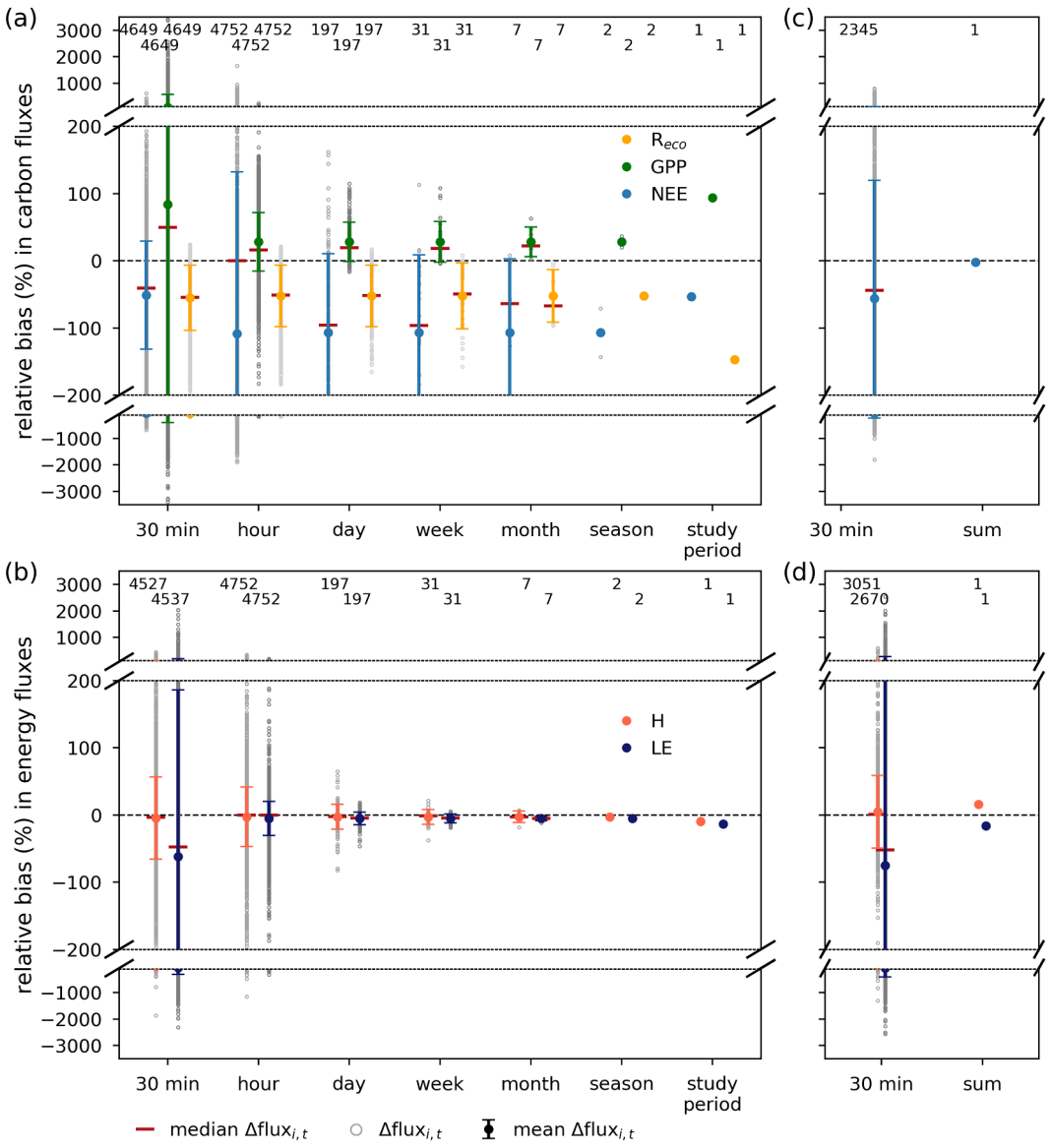

Fig. 7. Relative differences ($\Delta flux_{i,t}$ in %, cf. Eq. (1)) between 85 m- and two-level (a), (c) carbon flux and (b), (d) energy flux data in relation to the absolute mean flux of the entire study period for different time steps (subscripts i = varying, t = study period). $\Delta flux_{i,t}$ for only directly measured data (without gap-filling) are shown in panels (c) and (d). gray circles show all values of $\Delta flux_{i,t}$, colored dots with error bars indicate mean $\Delta flux_{i,t}$ with standard deviation, and red bars show medians (NEE: net ecosystem exchange, GPP: gross primary production, R_{eco}: ecosystem respiration, LE: latent heat flux, H: sensible heat flux). Numbers in each upper panel show the sample size for each time step.

Table 3
Cumulated sums of net ecosystem exchange (NEE), gross primary production (GPP), ecosystem respiration (R_{eco}), latent heat (LE), and sensible heat (H) flux estimates for the individual measurement levels and the two-level data for the study time period from September 2018 until July 2019, excluding the winter months November 2018-February 2019.

	85 m-level	Two-level	60 m-level
NEE (g C m^{-2})	-134	-64	-205
GPP (g C m^{-2})	-309	-431	-573
R_{eco} (g C m^{-2})	175	367	368
LE (MJ m^{-2})	324	341	416
H (MJ m^{-2})	426	438	514

were exchanged with the lower level measurements in the reference. Nevertheless, differences during daytime also occurred between data sets due to differences in gap-filled flux estimates.

Generally, the fluxes of NEE, R_{eco}, LE, and H were underestimated and that of GPP overestimated (Fig. 7). So, for GPP the absolute flux magnitude/CO_2 uptake was underestimated, and for NEE the fluxes measured at the single-level were always smaller and/or more negative than for the two-level approach (CO_2 release was underestimated and/or CO_2 uptake was overestimated). The relative difference in R_{eco} was almost constant throughout the day (Fig. S6 in supplementary material), because in the source partitioning approach the relationship between air temperature and R_{eco} was derived based on nighttime data and extrapolated to daytime. In half-hourly time steps the bias in R_{eco} was a magnitude smaller than in NEE or in GPP (not shown), but because the differences in R_{eco} between both data sets persisted throughout each day and not only appeared for a few half-hours, they summed up to a similar magnitude as ΔNEE or ΔGPP for one day or for the entire study period (Figs. 6, 7).

When using half-hourly data sets of a single-level on a tall tower, PBias (Eq. (2)) was largest in flux estimates, especially for GPP and LE (Fig. 8). PBias in half-hourly data was 66%, 325%, 57%, 160%, and 35%

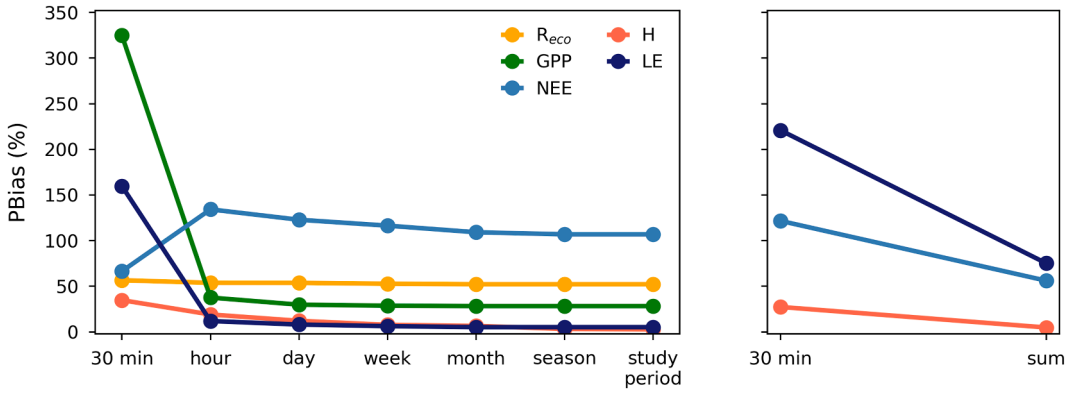

Fig. 8. (a) Mean absolute bias in relation to absolute reference mean (PBias, cf. Eq. (2)) for each flux for different time steps. The bias was calculated based on the difference between the single-level 85 m and the reference (two-level) data set. (b) PBias calculated with only directly measured data (without gap-filling) for the half-hourly time step and based on the sums of available data points (NEE: net ecosystem exchange, GPP: gross primary production, R_{eco}: ecosystem respiration, LE: latent heat flux, H: sensible heat flux).

for NEE, GPP, R_{eco}, LE, and H, respectively. The bias is smaller if aggregated data are used, where the aggregation to hourly time steps reduced PBias the most for GPP and LE. However, for NEE the PBias was relatively large. PBias in R_{eco} was the least dependent on selected time step due to the selected gap-filling method.

By excluding gap-filled data and only considering directly measured fluxes for half-hours with data points for both the single- and two-level approach, the mean $\Delta flux_{i,t}$ was similar to $\Delta flux_{i,t}$ for gap-filled data and the variance in $\Delta flux_{i,t}$ was still large (Figs. 7b, 7d, 8b). PBias was increased for NEE and LE. This shows that the here estimated relative bias and PBias were mostly introduced by flux footprint differences, because the magnitudes were similar between gap-filled and non-gap-filled data. Most studies using EC data consider gap-filled data sets for a long-term perspective, and our estimated biases provide a worst-case scenario for such studies (Figs. 7a, 7c, 8a). Here, two-level combination of the measurements impacted slightly the gap-filled data as can be seen in the diurnal courses of the fluxes in Figure S6 in the supplementary material. If the gap-filled data would be unaffected, the diurnal course of the two-level data would be congruent with the 85 m-level data during daytime and with the 60 m-level during nighttime, which is not the case here.

4. Discussion

4.1. Footprint variability

With the data combination of two EC measurement levels, we were able to quantify the bias in single-level measurements of carbon and energy fluxes over a heterogeneous landscape. However, the two-level approach did not improve the flux estimates during winter months. This was due to the fact that the stable atmospheric regimes prevailed throughout the entire day during winter conditions, and the diel variation of the averaged footprint area was therefore small at a single level (Figs. 3, 4, 5, Table 1). For the remaining study period, the footprint dimensions and area fractions of the different land cover types matched much better between day- and nighttime for the two-level data. During nighttime, the area fraction of forest increased with the two-level approach, resulting in a lower representation of clearcuts and peatlands, more similar to the daytime fraction, i.e. the diel variability was decreased (Figs. 3, 5).

Even though the two measurement heights at 85 m and 60 m were chosen deliberately to decrease the variability in footprints, the day- and nighttime footprints did not match perfectly. Other approaches of data set combination could be applied to decrease footprint variability. For instance, the atmospheric stability could be chosen as criterion, where during stable conditions data of the lower measurement height should be chosen. Another option would be to choose an optimal size of the footprint area (for instance here about 9 km^2), and then select for each half hour data of the level whose half-hourly footprint area is closest to this optimal size. However, frequent switching back and forth between measurement heights during the course of one day cannot be prevented with these two approaches. In this study, we focus on using day- and nighttime as the criterion for the data combination because these time periods can be derived easily and objectively without any gaps from standard radiation measurements and thus are independent of EC measurements.

Independent of the approach, the variation of the averaged footprint area and of the area fractions of the different land cover types can still be very large for shorter time scales (half-hourly, hourly, daily) due to frequent changes in wind direction and atmospheric stability. Hence, at shorter time scales, the fluxes are representative for differing surfaces and can still be biased. While we were unable to account for this bias source in this current study, our two-level approach is still applicable for shorter time scales since the footprint extensions will be aligned between day- and nighttime when there is no wind shear between both systems. By aggregating the data to longer time periods, the averaged footprint area becomes larger and representative for a wider range of surface elements and of the entire target area, and biases decrease.

Due to uncertain estimates of the roughness length (z_0) and boundary layer height (h_{bl}), bias may have been introduced to the footprint simulations. Kljun et al. (2015) conducted a sensitivity analysis for their FFP model towards the input parameters z_0 and h_{bl} for various stability conditions (see Section 6.1 in Kljun et al., 2015). They found only minor shifts and size alterations of the footprint by up to 3.7%, even for changes by ±20% for z_0 and h_{bl}. For stable conditions uncertain parameters have a higher impact than for non-stable conditions. The here conducted sensitivity analysis yielded also only small relative changes in the estimated seasonal footprint climatologies (Table 2). The footprint areas changed by up to 4.4% due to a change in h_{bl} by 10%, where a dependency on season or day- and nighttime could not be observed.

Considering shorter time steps, flux measurements can originate from different sinks and sources within the landscape, that not only differ in their general land cover type (forest, clearcut, or peatland), but also in canopy and soil characteristics, stand age, activity of heterotrophic organisms, albedo, net radiation, and other factors varying at a smaller spatial scale. For instance, Griebel et al. (2016) found directional differences in surface characteristics and weather patterns within their footprint, all of which affected measured fluxes and also influenced annual budgets. Even though we decreased the variabilities in the flux footprints and contributions from the various sinks and sources with the two-level combination, the heterogeneity within the landscape and so within the footprint areas was of course still given. This especially has an

impact on data analysis often applied to (half-)hourly data, such as gap-filling and source partitioning approaches, where relationships between physical drivers and obtained fluxes are derived for certain time periods and then applied to other time periods. The differences in footprint areas between the two time periods should be as small as possible.

4.2. Comparison of single- and two-level approach

The differences in measured nighttime fluxes at both levels (Fig. 2) already indicated that with the combination of daytime 85 m-level and nighttime 60 m-level data the flux amplitudes in the diel course would be changed. Due to the smaller nighttime fluxes in NEE and LE, also the sums of NEE and LE were smaller for the single-level than for the two-level data set (Table 3). Accordingly, the absolute sums were smaller for R_{eco} and GPP, because they were derived based on nighttime fluxes. Due to less negative/larger nighttime fluxes of H, it was assumed that its sum would be increased. However, the sum differed between the single- and two-level approach by less than 3%, because we excluded data from the winter months in our comparison of data sets and in the cumulated sums. Thus, the differing negative H fluxes were primarily excluded from the comparison.

By obtaining flux measurements on a single level, the footprint area increased during night compared to daytime. At our study site, this resulted in a decreased area fraction of forest while the area fractions of peatlands and clearcuts increased. Thus, the contribution to nighttime CO_2 release and evaporation by other land cover types than forest was increased, which resulted here in lower nighttime LE and NEE/R_{eco} than for the two-level approach. Deriving daytime R_{eco} based on this underestimated nighttime NEE, also yielded an underestimation of CO_2 uptake (less negative GPP) during the day. Hence, the bias in empirical and model analysis (e.g., gap-filling and source partitioning models) due to footprint variability should also be considered for the analysis of cumulated sums, budgets, and the ratios between CO_2 release and uptake.

On average for the various data time steps, the fluxes of NEE, R_{eco}, LE, and H were underestimated and those of GPP overestimated (less negative) with the single-level approach (Fig. 7). We found relative potential biases due to footprint variability ranging between 35% and 325% in our half-hourly data and up to 107% in cumulated sums (over 6 months; Fig. 8). However, for half-hourly, hourly, and daily data, seasonal differences could be observed (Fig. 6), where the footprint variability affected the measured carbon and energy fluxes the most during fall. Furthermore, bias estimates were very large for these shorter time intervals. Here, the distribution of our relative differences between the single- and two-level measurements (Fig. 7) showed that the carbon and energy fluxes could be both over- and underestimated by $> \pm 100\%$, especially in the half-hourly or hourly time steps, when using only one measurement level. This was also the case, when only measurements (excluding gap-filled data points) were compared for the half-hourly time steps with data available for the single- and two-level approach (Fig. 7c, 7d). These large over- and underestimations could have large implications for model-data fusion studies, where measurements that are not spatially representative are used to develop, calibrate and evaluate models, for site comparison studies, for up- or downscaling procedures, or for studies that only consider short time periods or intervals to investigate relations between environmental factors and fluxes.

Previous studies have estimated the magnitude of random errors in EC measurements. Hollinger et al. (2004) used concurrent measurements of two towers without overlapping footprint areas within a spruce-dominated forest to quantify the total random uncertainty, which includes also the instrument and turbulence sampling error next to the bias introduced by footprint variability. A comparison of half-hourly NEE, LE, and H suggested differences of 10-15% in their measurements of the two towers. The annual average net carbon uptake differed by $< 6\%$ (≈ 25 g C m^{-2} $year^{-1}$) between the two towers, which was also smaller than the interannual differences. Dragoni et al. (2007) obtained a random uncertainty of $< 4\%$ (< 12 g C m^{-2} $year^{-1}$) in their annual NEE estimate for a mixed deciduous forest. By conducting EC measurements on one tower in two heights (34 and 46 m) over a deciduous forest, Schmid et al. (2003) found a difference up to 80 g C m^{-2} in annual NEE (cf. Fig. 8 in Schmidt et al. 2003) between both systems. Additionally, they investigated the relative offset for hourly H between both systems, which was much smaller than for hourly NEE. Thus, Schmid et al. (2003) argue that differences in flux footprint variations are not likely an important factor, because the offset between both systems differed between NEE and H, and the patterns observed in the bias between both systems could not be explained with changes in wind direction. They assume that this offset was caused more likely by instrument and turbulence sampling errors. However, in our data set, we observed that changes in atmospheric stability and therefore footprint dimensions could explain differences in flux observations for two measurement heights, where wind shear between EC systems was negligible. The above cited studies quantified the total random uncertainty. To quantify the implications of surface heterogeneity (e.g., in leaf area index) on flux measurements separately (next to instrument error and uncertainty due to gap-filling), Oren et al. (2006) used flux data measured at six EC towers on ecosystem-level (with overlapping footprints) within a relatively homogeneous pine plantation. They found that even in such a homogeneous forest about 50% of uncertainty in half-hourly flux data and 6-49% in annual NEE can be linked to spatial variability in ecosystem activity (leaf area index, phenology, activity of heterotrophic organisms). This highlights the possible advantage of two-level measurements even in conventional EC studies to avoid bias due to footprint variations within the diel course.

To derive their optimized estimate for NEE of a heterogeneous mixed forest landscape, Davis et al. (2003) combined EC flux data of three different measurement heights (30, 122, and 396 m) on the WLEF television tower. Depending on atmospheric stability, boundary layer depth, and data availability, they chose measurements from a certain level for their final data set to decrease the change in the footprint area, to increase data coverage, and to minimize the influence of a clearing with a 200 m radius around their tower base. Daily NEE estimates only using one measurement level lay within a 20% range of the optimized NEE estimate (Davis et al., 2003). In this bias estimate only hours with data available for all three levels and during summer months were included. We chose day- and nighttime as the criterion for the data combination (and not atmospheric stability and data availability as Davis et al., 2003) because these time periods can be derived easily without any gaps and independent of EC measurements. In our approach, the distance between our measurement levels was chosen deliberately to obtain matching day- and nighttime footprints, and was much smaller than in the set-up of Davis et al. (2003). It is also noteworthy that our approach further benefitted from gathering a-prior footprint area estimates based on wind data to ensure a good match between the two levels.

Uncertainties introduced by the different instrumental set-up between both measurement heights affected the comparison of the single- and two-level approach. The here applied correction of the CO_2 and H_2O raw data in reference to the vertical profile system (Section 2.3.1) yielded lower PBias for this data analysis than when this correction was not applied prior to flux processing (not shown). This confirms that some difference due to the instrumental difference was corrected. Mean relative differences between the 85 m- and 60 m-level data were about 61%, 48%, and 12% for NEE, LE, and H, respectively, for half-hourly data obtained during optimal meteorological conditions (cf. Appendix B). The estimated PBias between both levels and the 85 m-level taken as reference were 59%, 37%, and 15% for NEE, LE, and H, respectively, which are for the energy fluxes much lower than the PBias of the single- and two-level comparisons for half-hourly data shown in Fig. 8. For NEE, PBias between both levels was only slightly smaller in

half-hourly fluxes than for the single- and two-level comparison. However, considering aggregated fluxes (hourly to seasonal) PBias increased for the latter comparison (Fig. 8). Further, the here applied correction of the CO_2 and H_2O raw data in reference to the vertical profile system (Section 2.3.1) and thus, an alignment of the gas analyzers of both measurement levels yielded lower PBias for this data analysis than when this correction was not applied prior to flux processing. Thus, the here estimated absolute relative bias introduced by obtaining flux measurements on a single level were mostly caused by the higher flux footprint variability, and to a much lesser extent by instrumental differences, but unfortunately, they could not be excluded entirely.

Additionally, uncertainties in flux data can be induced by the applied quality check, gap-filling and source partitioning approaches (e.g., Oren et al., 2006, Schmid et al., 2003), where large data gaps even increase these uncertainties, especially when they occur during time periods of difficult measurement conditions (e.g., low temperature and icing of instruments) and with fluxes of low magnitude and low variation (less active ecosystem). Further, periods of lower EC data quality due to low turbulence, stable atmospheric regimes, and liquid water in tubes usually prevail during night and/or winter. Here, we assumed that these uncertainties are given for all used EC data sets and are of similar magnitude at both levels, because the same approaches were always used, making the data sets comparable. Further, data obtained during winter months was excluded from the comparison of the single- and two-level approach, thus, mostly excluding periods with low turbulence and harsh conditions. Moreover, we minimized the bias in the flux estimates introduced by possible advection processes by filtering out periods with prevailing vertical or horizontal advection fluxes after Wharton et al. (2009) and by applying storage term corrections. However, uncertainties in the flux estimates of both EC systems due to the chosen flux processing scheme, quality checks, gap-filling strategies, source partitioning methods, and instrumental set-ups could not be eradicated completely.

Next to possible large implications for model-data fusion studies, site comparison studies, up- or downscaling procedures, or for studies using only short time periods and/or scales, the footprint variability affects also the extrapolation of nighttime NEE—temperature relationships to daytime, as done in various source partitioning, gap-filling or model approaches.

5. Conclusions

By combining data from two EC measurement levels, we quantified the bias in single-level measurements of carbon and energy flux estimates for various time scales over a heterogeneous landscape. Our study showed that by choosing measurements of the higher level during daytime and of the lower level during nighttime, the diel variation in the averaged footprint area was decreased significantly. However, during winter months diel footprint variability remained small at a given measurement level, because stable atmospheric regimes prevailed throughout the entire day. Thus, the footprint variability could not be decreased with this two-level approach during winter.

Our study revealed potential biases due to footprint variability over heterogeneous terrain up to 160% in the half-hourly NEE, LE, and H fluxes from this study site and up to 5% in cumulated sums (over 6 months) of energy fluxes and even 107% in cumulated sums in NEE. Furthermore, the distribution of our relative differences between the single- and two-level measurements showed that the carbon and energy fluxes could be over- or underestimated by $>$ 100%, especially in the half-hourly or hourly time steps, by using only one measurement level. This could have large implications for model-data fusion studies, site comparison studies, up- or downscaling procedures, analysis of relations between environmental factors and fluxes, or for studies that only consider short time periods or intervals. Furthermore, the sink and source strengths of certain ecosystems could be misinterpreted.

Especially for high EC measurement heights, the variation of the averaged footprint area within the diel course and hence the bias can become very large. Moreover, the bias depends on the degree of heterogeneity of the target area and the distribution of scalar sinks and sources, and thus, could become very important for EC systems on stand/ecosystem-level and/or for study sites with a high diel variability in atmospheric stability. Besides decreasing the bias in flux observations due to variable flux footprints, the two-level approach could also provide a good data basis for gap-filling fluxes between the two EC systems.

Declaration of Competing Interest

The authors declare that they have no known competing financial interests or personal relationships that could have appeared to influence the work reported in this paper.

Data availability

Data will be made available on request.

Acknowledgments

This research was supported by the Kempe Foundation [Grant #JCK-1815], by the Swedish Research Council for Environment, Agricultural Sciences and Spatial Planning (FORMAS) [Grant #942-2015-49], the Swedish Research Council, and contributing research institutes to the Swedish Integrated Carbon Observation System (ICOS-Sweden) Research Infrastructure and the Swedish Infrastructure for Ecosystem Science (SITES). This research contributes also to the Strategic Research Area: ModElling the Regional and Global Earth system, MERGE, funded by the Swedish government. Further, JC acknowledges funding from Kempe Foundation [Grant #SMK-1743] and Center for Ocean Research in Hong Kong and Macau (CORE). We thank the staff from the Svartberget Field Station, especially Per Marklund, Paul Smith, and Giuseppe De Simon, for their continuous support in data acquisition and instrument maintenance. We also thank Jutta Holst (INES, Lund University) for her ICOS data support. Finally, we thank the reviewers for their helpful and constructive comments that improved the quality of this paper.

Supplementary materials

Supplementary material associated with this article can be found, in the online version, at doi:10.1016/j.agrformet.2023.109523.

Appendix A

Table A1 and A2

Table A1
Absolute limits applied to each variable for quality-check (NEE: net ecosystem exchange, LE: latent heat flux, H: sensible heat flux).

Variable		Absolute min	Absolute max
CO_2 mixing ratio	ppm	350	450
H_2O mixing ratio	ppt	0	30
NEE	µmol m^{-2} s^{-1}	-30	30
LE	W m^{-2}	-150	500
H	W m^{-2}	-300	750
CO_2 storage term	µmol m^{-2} s^{-1}	-25	25
LE storage term	W m^{-2}	-200	200
H storage term	W m^{-2}	-200	200

Table A2
Relative fraction of gaps (%) in entire data set (15,264 30 min-time periods) of processed half-hourly fluxes and added due to various quality-checks for each flux variable and eddy covariance system (NEE: net ecosystem exchange, LE: latent heat flux, H: sensible heat flux).

	—— 85 m-level ——			—— 60 m-level ——		
	NEE	H	LE	NEE	H	LE
In processed half-hourly fluxes	10.1	10.1	10.1	16.0	15.9	16.4
Due to filtering quality flag=2	22.3	10.9	8.8	10.4	7.9	12.2
Due to filtering absolute limits	1.7	2.5	2.1	1.7	2.5	1.7
Due to too low boundary layer height	4.0	4.3	5.1	3.3	3.6	3.5
Due to wind distortion, maintenance, malfunction	2.5	2.8	2.7	2.4	2.3	2.4
Due to filtering for advection/low turbulence	11.7	13.6	14.5	10.5	11.0	9.9
Due to despiking	3.3	1.5	4.2	4.4	1.2	4.5
Due to complete quality check	45.4	35.6	37.4	32.8	28.5	34.2
Total fraction of gaps	55.5	45.7	47.5	48.7	44.4	50.6

Appendix B

Eddy covariance instrument comparison

To make sure that the observed differences between the two eddy covariance (EC) systems at 85 m and 60 m measurement height were caused by the differing source areas and not by instrumental differences, an instrument comparison of the gas analyzers and sonic anemometers was conducted. Unfortunately, it was not logistically possible to install both EC systems next to each other at the same height for a short time period, which would have been optimal. Thus, we compared measurements of both EC systems which were obtained under similar and optimal conditions and of (presumably) similar flux footprints (Fig. B1). Following the parameterization of the flux footprint prediction model after Kljun et al. (2015), the footprint depends on measurement height, roughness length, wind direction, wind velocity, friction velocity, Obukhov length (atmospheric stability), standard deviation of the lateral wind component, and planetary boundary layer height. For the instrument comparison, we chose data from May until mid-July 2019 of both EC systems, where the difference between measured wind directions of both EC systems was $< 10^{\circ}$, the difference in mean wind velocities < 1 m s^{-1}, in friction velocities < 0.1 m s^{-1}, in Obukhov lengths < 50 m, and in standard deviations of the lateral wind velocity < 0.2 m s^{-1}. The roughness length and boundary layer height were identical for both EC systems. Also, time periods with precipitation were discarded. However, the extent of the corresponding footprints still differed between both EC systems because of the large difference in measurement heights. The relative area fractions of forest, clearcuts, or peatlands within the footprint (80% footprint flux contribution) differed only up to 3.4% between the 85 m- and 60 m-level EC system.

Furthermore, we aligned the concentration measurements of both gas analyzers in reference to the measurements of the vertical profile. The CO_2 measurements of the vertical profile system were beforehand validated based on the ICOS atmospheric system, because the latter was calibrated frequently and extensively. First, the half-hourly CO_2 and H_2O measurements were compared between the profile system (reference) and each EC system. The absolute offset between the reference and the EC system time series was estimated by taking the difference of the rolling means of the concentration with a window of seven days. Secondly, time steps of similar and optimal conditions (see above) between both EC systems were chosen during the entire study period—to ensure relative similar source areas. Thirdly, regressions were derived between the reference and each EC system for CO_2 and H_2O with the reduced major axis regression method. Fourthly, based on these estimated offsets and regressions the CO_2 and H_2O raw data (10 Hz data) were corrected and then fluxes were reprocessed with EddyPro®.

Fig. B1 shows the comparison between both levels for the variance of the vertical wind component (σ_w^2), sensible heat flux (H), sonic temperature (T_s), and its variance ($\sigma_{T_s}{}^2$), all measured by the sonic anemometers, and for the deviations of the mixing ratios from the mean concentrations ($\Delta\chi_{CO_2}$, $\Delta\chi_{H_2O}$), CO_2 flux (F_{CO_2}), and latent heat flux (LE), all measured by the gas analyzers, from May until mid-July 2019. The correlations of most variables improved when similar meteorological conditions (large plots) were considered in comparison to the complete data sets (inner, smaller plots). However, discrepancies were still visible, especially in T_s and gas concentration measurements. In general, we can expect a difference in all variances and absolute magnitudes of T_s due to the difference in measurement heights. The variances of w and T_s should decrease with height due to the increasing eddy sizes. After Prueger and Kustas (2005), the roughness sublayer is about 1.5-3.5 times as high as the vegetation or obstacles, and above the surface sublayer extends up to 100 m. With an average canopy height of 23 m within the annual footprint and a maximum tree height of about 30 m, the two EC systems in 85 m and 60 m would lay somewhere between the roughness and surface sublayer during daytime. The surface sublayer is fully turbulent, directly influenced by mechanical and buoyancy forcings from the surface, and wind speed profiles are generally logarithmic under neutral conditions. Furthermore, fluxes can be assumed to be nearly constant with height, so that flux differences between two measurement heights

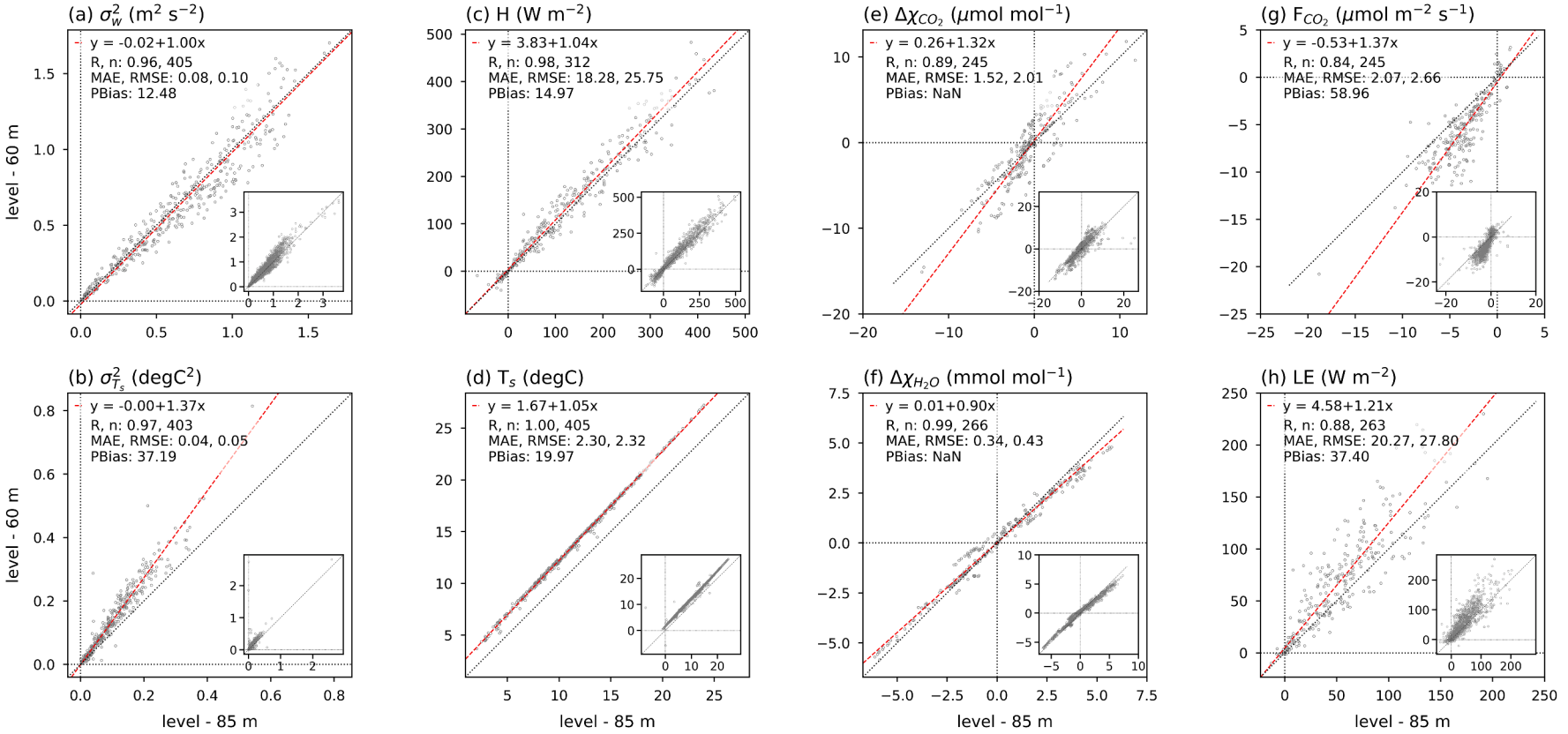

Fig. B1. Data comparison of both eddy covariance systems at 85 m and 60 m height obtained during similar and optimal conditions (see description in text) from May until mid-July 2019. Comparisons are shown for (a) the variance of the vertical wind component (σ_w^2), (b) variance of the sonic temperature ($\sigma_{T_s}{}^2$), (c) sensible heat flux (H), (d) sonic temperature (T_s), (e, f) the deviations of the mixing ratios from the rolling mean concentrations with a seven day window ($\Delta\chi_{CO_2}$, $\Delta\chi_{H_2}O$), (g) CO_2 flux (F_{CO_2}), and (h) latent heat flux (LE). For this comparison, H, LE, and F_{CO_2} were not storage corrected. Also, equations of the reduced major axis regression, correlation coefficient (R), sample size (n), mean absolute error (MAE), root mean square error (RMSE), and relative potential bias (PBias) between both data sets are shown for each comparison. The inner smaller plots show the correlation of both unfiltered data sets for all meteorological conditions from May until mid-July 2019.

result from different footprints or upwind source areas. Following this, the flux measurements of NEE, LE, and H obtained under the above defined meteorological conditions should be almost identical. Because of occasional influence of the roughness sublayer (when the lower sensor is within), the scatter in the comparison of both measurement levels can be increased. A comparison of fluxes between both measurement levels depending on prevailing wind direction and roughness sublayer height (given by surface roughness and tree height) showed only non-significant differences (not shown). Here, the mean absolute errors and root mean square errors were relatively small for NEE, LE, and H. However, the linear regressions show discrepancies between measurement heights. The larger differences in NEE and LE indicated by the regression line's slope could be caused by the longer tube length for the 85 m-level EC system than for the 60 m-level EC system. Mean relative differences between the 85 m- and 60 m-level data were about 61%, 48%, and 12% for NEE, LE, and H, respectively. Overall, the variance of vertical wind speed and the CO_2 and H_2O mixing ratios are of main interest for EC measurements and they show a satisfactory comparison (Fig. B1a, B1e, B1f). Still, due to the long tube the 85 m-level EC system underestimates especially NEE and LE, where the applied time lag optimization and spectral corrections can only partly reduce the measurement errors.

For this instrument comparison, we also estimated the relative potential bias (PBias) as described in Eq. (2) for the half-hourly time steps. As can be seen in Fig. B1, PBias was smaller in this instrument comparison than for the final gap-filled data as stated in the Results Section 3.3. Thus, we conclude that the larger relative differences we see in our final results between the single- and two-level data set were indeed caused by the higher flux footprint variability in the single-level measurements, and to a lesser extent by instrumental differences.

Appendix C

Comparison of data obtained with heated and non-heated sonic anemometers

During winter, the sonic anemometers were heated at our study site to prevent ice or snow on the instruments, when air temperature and humidity fell below a certain threshold. In this study, data points obtained during activated heating were not discarded before flux calculation to avoid large data gaps, because up to about 13% of the half-hourly flux data during our study period would have been additionally filtered out, especially nighttime data. Goodrich et al. (2016) and Kittler et al. (2017) analyzed flux data obtained with heated and non-heated anemometers in cold climate conditions and concluded that temperature measurements and sensible heat flux (H) were overestimated by the heated system, and the variance of the vertical wind component (σ_w^2) was influenced less, but the effect on scalar fluxes and annual carbon balances was small. Here, we like to analyze the influence of anemometer heating of the two tall tower eddy covariance (EC) systems and to estimate the relating uncertainty by comparing the turbulence data to the ICOS EC system at 34.5 m measurement height. The anemometer (Gill HS-50, Gill Instruments Ltd, Lymington, UK) of this ICOS EC system was heated only periodically (about every four hours for less than one hour during winter) and thus, has a much higher data coverage and a presumably smaller bias in wind components (Goodrich et al., 2016) than the tall tower EC systems. For the ICOS EC system, flux raw data were processed with the EddyPro® Software (v7.0.6) following closely the ICOS protocol (Sabbatini et al., 2018), while data obtained with activated sonic anemometer heating was always discarded. A few adjustments compared to Sabbatini et al. (2018) have been made: For the raw data quality check, the absolute limits of sonic temperature (T_s) were adjusted to the local plausible range and to the operating temperature range of the gas analyzers (-30 °C to +40 °C). The double rotation method was used for the anemometer tilt correction, for the high-frequency spectral correction, the approach after Ibrom et al. (2007) was applied (Rebmann et al., 2012). The post-processing data quality-check was performed as described in Section 2.3.3.

In Fig. C1, the correlations of σ_w^2, friction velocity (u_*), H, T_s, and its variance ($\sigma_{T_s}{}^2$) between the high-quality data of the ICOS EC system and the tall tower EC systems are shown. We compared data clouds obtained with non-heated (gray dots) and heated anemometers (black dots) of the tall tower EC systems measured during the winter period (October 2018-April 2019) (data obtained with a heated anemometer of the ICOS EC system was always discarded). If the regression lines of these two data clouds in each diagram are similar, then the influence of the anemometer heating was low.

The sample sizes of the heated data were always smaller than of the non-heated data independent of the variable, which has an influence on the correlation coefficients. The slopes of the regression lines differed from 1.00 due to the difference in measurement height between the EC systems. The variables of the turbulent wind field, σ_w^2 and u_*, compared well between heated and non-heated anemometer data, where the regression line slopes were very similar and offsets were always close to zero (Fig. C1a, b). But the slightly decreased slopes due to activated heating indicate an underestimation of the wind field components, which contradicts the observations of Goodrich et al. (2016) and Kittler et al. (2017).

The temperature measurements did not compare as well between data sets (Fig. C1c, d, e). In T_s (Fig. C1c) an instrument artifact of the Gill sonic anemometer of the ICOS EC system is visible, where the relationship between very low air temperatures changes abruptly (light-gray dots; cf. Mauder et al., 2007). This change in the slope is not visible in the correlation between the two tall tower EC systems (CSAT3 3-D versus METEK uSonic-3 Omni sonic anemometer; not shown). Thus, in the following comparison of T_s, H, and $\sigma_{T_s}{}^2$, we only considered data points when T_s of the ICOS EC system was > 3 °C (Fig. C1c, d, e), which improved the comparisons significantly. While the tall tower anemometers were heated, mostly a negative H and small T_s were measured, while during deactivated heating also relatively large positive H and high T_s were observed (Fig. C1d). The regression lines for H compared relatively well considering the differing magnitudes of H between activated and deactivated heating. The skewness of and the scatter in $\sigma_{T_s}{}^2$ were generally very large for heated and non-heated data, so that we ln-transformed the data for a better comparison (Fig. C1e).

The sonic anemometer heating introduced an additional uncertainty in our measurements (next to uncertainties due to instrumental differences and applied methods for gap-filling and source partitioning), but in our opinion it is very small. Furthermore, our analysis focused on data obtained mostly during months, where sonic anemometer heating was not necessary. For instance, by excluding the winter months, only 423 and 24 half-hourly NEE measurements were obtained during activated sonic anemometer heating by the 60 m- and 85 m-level EC systems, respectively.

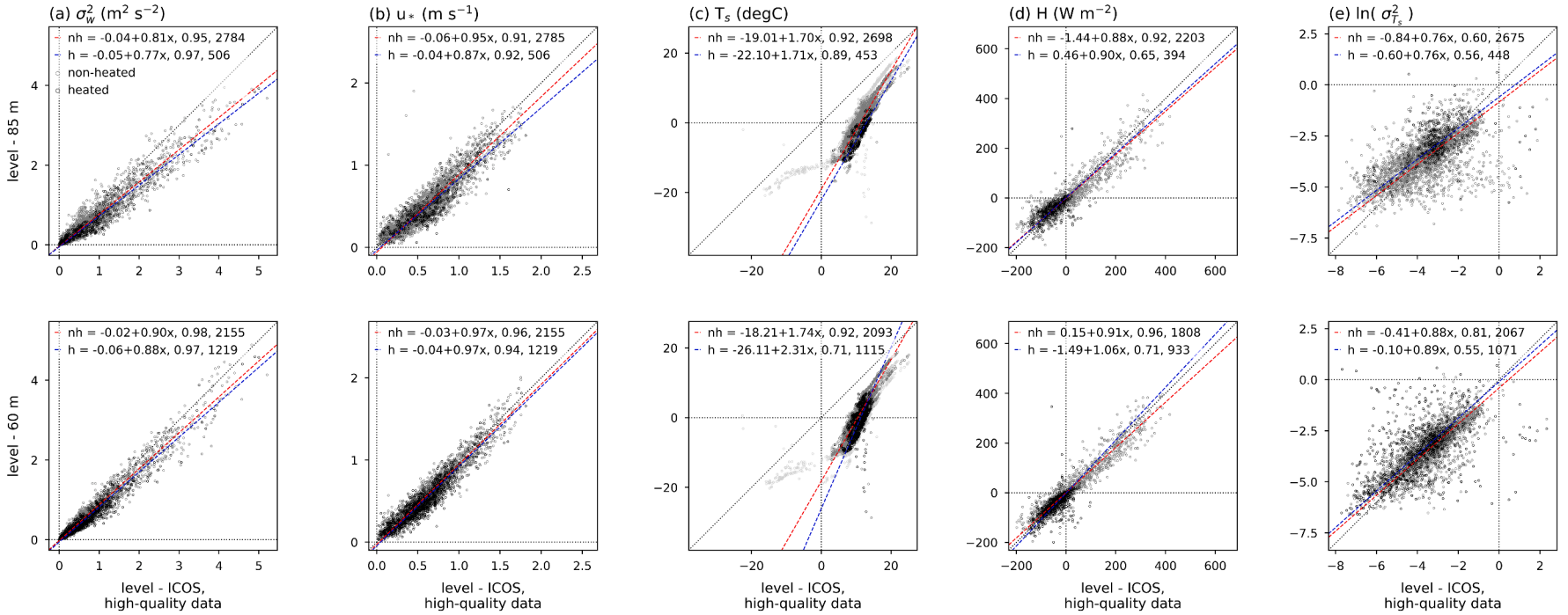

Fig. C1. Comparison of data obtained from the ecosystem-level ICOS eddy covariance (EC) system and both tall tower EC systems (85 m and 60 m) for half-hours without (gray dots, red regression line) and with (black dots, blue regression line) activated sonic anemometer heating between October 2018 and April 2019. All data are quality-checked and data of the ICOS EC system always excludes half-hours with activated anemometer heating. The columns show from left to right (a) variance of the vertical wind velocity (σ_w^2), (b) friction velocity (u_*), (c) sonic temperature (T_s), (d) sensible heat flux (H; not storage term corrected), and (e) ln-transformed variance of T_s ($\sigma_{T_s}^2$). Equations of each reduced major axis regression (nh: non-heated, h: heated), correlation coefficient, and sample size are listed in this order. In (c), the original T_s data are shown (light-gray dots) showing an instrumental artifact of the sonic anemometer at 34.5 m (cf. Mauder et al., 2007). Data of H, T_s, and $\sigma_{T_s}^2$ were discarded for half-hours when T_s of the ICOS EC system was < 3 °C for a better comparison.

Appendix D

Estimation of d and z_0 based on two wind profile equations

The zero-plane displacement height (d) and roughness length (z_0) are needed as input parameters (amongst others) for the flux footprint prediction model after Kljun et al. (2015). Under near-neutral conditions (stability correction factor drops out under neutral conditions) the following logarithmic wind profile equation can be assumed to be valid:

$$\leftrightarrow \overline{u}(z) = \frac{u_*}{\kappa} \cdot \ln\left(\frac{z-d}{z_0}\right) \tag{D1}$$

where $\overline{u}(z)$ (m s^{-1}) is the mean horizontal wind velocity at measurement height z (m), u_* (m s^{-1}) is the friction velocity, and κ (-) is the von Karman constant ($\kappa = 0.4$). Eq. (D1) can be rearranged to:

$$z_0 = \frac{z-d}{\exp\left(\overline{u}(z) \cdot \frac{\kappa}{u_*}\right)}$$

and

$$d = z - z_0 \cdot \exp\left(\overline{u}(z) \cdot \frac{\kappa}{u_*}\right).$$

Because of the heterogeneity of the boreal landscape, d and z_0 were estimated for each 30°-sector of wind direction (Chi et al., 2019) with the turbulence measurements of the 60 m-level EC system and the ICOS EC system at 34.5 m. Here, the logarithmic wind profile equations relating to the two measurement heights z_1 and z_2 were equated for d or z_0, respectively (Eq. (D2), D4), then solved for the other parameter (Eq. (D3), D5), and finally the resulting median within a reasonable range was selected for d and z_0, respectively.

$$\leftrightarrow \frac{z_1-d}{\exp\left(\overline{u}_1(z_1) \cdot \frac{\kappa}{u_{*1}}\right)} = \frac{z_2-d}{\exp\left(\overline{u}_2(z_2) \cdot \frac{\kappa}{u_{*2}}\right)} \tag{D2}$$

$$\leftrightarrow d = \frac{z_1 \cdot \exp\left(\overline{u}_2(z_2) \cdot \frac{\kappa}{u_{*2}}\right) - z_2 \cdot \exp\left(\overline{u}_1(z_1) \cdot \frac{\kappa}{u_{*1}}\right)}{\exp\left(\overline{u}_2(z_2) \cdot \frac{\kappa}{u_{*2}}\right) - \exp\left(\overline{u}_1(z_1) \cdot \frac{\kappa}{u_{*1}}\right)} \tag{D3}$$

$$\leftrightarrow z_1 - z_0 \cdot \exp\left(\overline{u}_1(z_1) \cdot \frac{\kappa}{u_{*1}}\right) = z_2 - z_0 \cdot \exp\left(\overline{u}_2(z_2) \cdot \frac{\kappa}{u_{*2}}\right) \tag{D4}$$

$$\leftrightarrow z_0 = \frac{z_1 - z_2}{\exp\left(\overline{u}_1(z_1) \cdot \frac{\kappa}{u_{*1}}\right) - \exp\left(\overline{u}_2(z_2) \cdot \frac{\kappa}{u_{*2}}\right)} \tag{D5}$$

Only data obtained under near-neutral atmospheric stability with -0.1 < *(z-d)*/L < 0.07 (with $d = 2/3 \bullet$ canopy height), with wind velocities of the lowest (above canopy) measurement height > 4 m s^{-1} (after Sogachev and Dellwik 2017), and with wind velocities of the higher measurement height larger than of the lower one were used. With this approach, we found values for d between 17.2 m and 28.4 m and z_0 between 0.8 m and 2.8 m for the various 30°-sector of wind direction. The resulted wind profiles are shown in Fig. S11 in supplementary material.

References

Baker, I., Denning, A.S., Hanan, N., Prihodko, L., Uliasz, M., Vidale, P.L., Davis, K., Bakwin, P., 2003. Simulated and observed fluxes of sensible and latent heat and CO_2 at the WLEF-TV tower using SiB2.5. Glob. Chang. Biol. 9, 1262–1277. https://doi.org/10.1046/j.1365-2486.2003.00671.x.

Barcza, Z., Kern, A., Haszpra, L., Kljun, N., 2009. Spatial representativeness of tall tower eddy covariance measurements using remote sensing and footprint analysis. Agric. For. Meteorol. 149, 795–807. https://doi.org/10.1016/j.agrformet.2008.10.021.

Berger, B.W., Davis, K.J., Yi, C., 2001. Long-term carbon dioxide fluxes from a very tall tower in a northern forest: flux measurement methodology. J. Atmosp. Ocean. Technol. 18, 529–542. https://doi.org/10.1175/1520-0426(2001)018<0529:LTCDFF>2.0.CO;2.

Butterworth, B.J., Desai, A.R., Metzger, S., Townsend, P.A., Schwartz, M.D., Petty, G.W., Mauder, M., Vogelmann, H., Andresen, C.G., Augustine, T.J., Bertram, T.H., Brown, W.O.J., Buban, M., Cleary, P., Durden, D.J., Florian, C.R., Iglinski, T.J., Kruger, E.L., Lantz, K., Lee, T.R., Meyers, T.P., Mineau, J.K., Olson, E.R., Oncley, S. P., Paleri, S., Pertzborn, R.A., Pettersen, C., Plummer, D.M., Riihimaki, L.D., Ruiz Guzman, E., Sedlar, J., Smith, E.N., Speidel, J., Stoy, P.C., Sühring, M., Thom, J.E., Turner, D.D., Vermeuel, M.P., Wagner, T.J., Wang, Z., Wanner, L., White, L.D., Wilczak, J.M., Wright, D.B., Zheng, T., 2021. Connecting land-atmosphere interactions to surface heterogeneity in CHEESEHEAD19. Bull. Am. Meteorol. Soc. 102, E421–E445. https://doi.org/10.1175/BAMS-D-19-0346.1.

Chapin III, F.S., Woodwell, G.M., Randerson, J.T., Rastetter, E.B., Lovett, G.M., Baldocchi, D.D., Clark, D.A., Harmon, M.E., Schimel, D.S., Valentini, R., Wirth, C., Aber, J.D., Cole, J.J., Goulden, M.L., Harden, J.W., Heimann, M., Howarth, R.W., Matson, P.A., McGuire, A.D., Melillo, J.M., Mooney, H.A., Neff, J.C., Houghton, R.A., Pace, M.L., Ryan, M.G., Running, S.W., Sala, O.E., Schlesinger, W.H., Schulze, E.D., 2006. Reconciling carbon-cycle concepts, terminology, and methods. Ecosystems 9, 1041–1050. https://doi.org/10.1007/s10021-005-0105-7.

Chi, J., Nilsson, M.B., Kljun, N., Wallerman, J., Fransson, J.E.S., Laudon, H., Lundmark, T., Peichl, M., 2019. The carbon balance of a managed boreal landscape measured from a tall tower in northern Sweden. Agric. For. Meteorol. 274, 29–41. https://doi.org/10.1016/j.agrformet.2019.04.010.

Chi, J., Nilsson, M.B., Laudon, H., Lindroth, A., Wallerman, J., Fransson, J.E.S., Kljun, N., Lundmark, T., Ottosson-Löfvenius, M., Peichl, M., 2020. The net landscape carbon balance – Integrating terrestrial and aquatic carbon fluxes in a managed boreal forest landscape in Sweden. Glob. Change Biol. 26, 2353–2367. https://doi.org/10.1111/gcb.14983.

Chu, H., Luo, X., Ouyang, Z., Chan, W.S., Dengel, S., Biraud, S.C., Torn, M.S., Metzger, S., Kumar, J., Arain, M.A., Arkebauer, T.J., Baldocchi, D., Bernacchi, C., Billesbach, D., Black, T.A., Blanken, P.D., Bohrer, G., Bracho, R., Brown, S., Brunsell, N.A., Chen, J., Chen, X., Clark, K., Desai, A.R., Duman, T., Durden, D., Fares, S., Forbrich, I., Gamon, J.A., Gough, C.M., Griffis, T., Helbig, M., Hollinger, D., Humphreys, E., Ikawa, H., Iwata, H., Ju, Y., Knowles, J.F., Knox, S.H., Kobayashi, H., Kolb, T., Law, B., Lee, X., Litvak, M., Liu, H., Munger, J.W., Noormets, A., Novick, K., Oberbauer, S.F., Oechel, W., Oikawa, P., Papuga, S.A., Pendall, E., Prajapati, P., Prueger, J., Quinton, W.L., Richardson, A.D., Russell, E.S., Scott, R.L., Starr, G., Staebler, R., Stoy, P.C., Stuart-Haëntjens, E., Sonnentag, O., Sullivan, R.C., Suyker, A., Ueyama, M., Vargas, R., Wood, J.D., Zona, D., 2021. Representativeness of eddy-covariance flux footprints for areas surrounding AmeriFlux sites. Agric. For. Meteorol. 301-302, 108350 https://doi.org/10.1016/j.agrformet.2021.108350.

Davis, K.J., Bakwin, P.S., Yi, C., Berger, B.W., Zhao, C., Teclaw, R.M., Isebrands, J.G., 2003. The annual cycles of CO_2 and H_2O exchange over a northern mixed forest as

observed from a very tall tower. Glob. Change Biol. 9, 1278–1293. https://doi.org/10.1046/j.1365-2486.2003.00672.x.
Desai, A.R., 2010. Climatic and phenological controls on coherent regional interannual variability of carbon dioxide flux in a heterogeneous landscape. J. Geophys. Res. 115, G00J02. https://doi.org/10.1029/2010JG001423.
Desai, A.R., Moorcroft, P.R., Bolstad, P.V., Davis, K.J., 2007. Regional carbon fluxes from an observationally constrained dynamic ecosystem model: impacts of disturbance, CO_2 fertilization, and heterogeneous land cover. J. Geophys. Res. 112, G010117 https://doi.org/10.1029/2006JG000264.
Desai, A.R., Noormets, A., Bolstad, P.V., Chen, J., Cook, B.D., Davis, K.J., Euskirchen, E. S., Gough, C., Martin, J.G., Ricciuto, D.M., Schmid, H.P., Tang, J., Wang, W., 2008. Influence of vegetation and seasonal forcing on carbon dioxide fluxes across the Upper Midwest, USA: implications for regional scaling. Agric. For. Meteorol. 148, 288–308. https://doi.org/10.1016/j.agrformet.2007.08.001.
Desai, A.R., Xu, K., Tian, H., Weishampel, P., Thom, J., Baumann, D., Andrews, A.E., Cook, B.D., King, J.Y., Kolka, R., 2015. Landscape-level terrestrial methane flux observed from a very tall tower. Agric. For. Meteorol. 201, 61–75. https://doi.org/10.1016/j.agrformet.2014.10.017.
Donnelly, A., Yu, R., Liu, L., Hanes, J.M., Liang, L., Schwartz, M.D., Desai, A.R., 2019. Comparing in-situ leaf observations in early spring with flux tower CO_2 exchange, MODIS EVI and modeled LAI in a northern mixed forest. Agric. For. Meteorol. 278, 107673 https://doi.org/10.1016/j.agrformet.2019.107673.
Dragoni, D., Schmid, H.P., Grimmond, C.S.B., Loescher, H.W., 2007. Uncertainty of annual net ecosystem productivity estimated using eddy covariance flux measurements. J. Geophys. Res. 112, D17102. https://doi.org/10.1029/2006JD008149.
Gelybó, G., Barcza, Z., Kern, A., Kljun, N., 2013. Effect of spatial heterogeneity on the validation of remote sensing based GPP estimations. Agric. For. Meteorol. 174-175, 43–53. https://doi.org/10.1016/j.agrformet.2013.02.003.
Giannico, V., Chen, J., Shao, C., Ouyang, Z., John, R., Lafortezza, R., 2018. Contributions of landscape heterogeneity within the footprint of eddy-covariance towers to flux measurements. Agric. For. Meteorol. 260-261, 144–153. https://doi.org/10.1016/j.agrformet.2018.06.004.
Goodrich, J.P., Oechel, W.C., Gioli, B., Moreaux, V., Murphy, P.C., Burba, G., Zona, D., 2016. Impact of different eddy covariance sensors, site set-up, and maintenance on the annual balance of CO_2 and CH_4 in the harsh Arctic environment. Agric. For. Meteorol. 228-229, 239251 https://doi.org/10.1016/j.agrformet.2016.07.008.
Griebel, A., Bennett, L.T., Metzen, D., Cleverly, J., Burba, G., Arndt, S.K., 2016. Effects of inhomogeneities within the flux footprint on the interpretation of seasonal, annual, and interannual ecosystem carbon exchange. Agric. For. Meteorol. 221, 50–60. https://doi.org/10.1016/j.agrformet.2016.02.002.
Hersbach, H., Bell, B., Berrisford, P., Biavati, G., Horányi, A., Muñoz Sabater, J., Nicolas, J., Peubey, C., Radu, R., Rozum, I., Schepers, D., Simmons, A., Soci, C., Dee, D., Thépaut, J.N. (2018): ERA5 hourly data on single levels from 1979 to present. Copernicus Climate Change Service (C3S) Climate Data Store (CDS). Accessed on 09 July 2020, doi: 10.24381/cds.adbb2d47.
Hollinger, D.Y., Aber, J., Dail, B., Davidson, E.A., Goltz, S.M., Hughes, H., Leclerc, M.Y., Lee, J.T., Richardson, A.D., Rodrigues, C., Scott, N.A., Achuatavarier, D., Walsh, J., 2004. Spatial and temporal variability in forest-atmosphere CO_2 exchange. Glob. Change Biol. 10, 1689–1706. https://doi.org/10.1111/j.1365-2486.2004.00847.x.
Ibrom, A., Dellwik, E., Flyvbjerg, H., Jensen, N.O., Pilegaard, K., 2007. Strong low-pass filtering effects on water vapour flux measurements with closed-path eddy correlation systems. Agric. For. Meteorol. 147, 140–156. https://doi.org/10.1016/j.agrformet.2007.07.007.
Keppel-Aleks, G., Wennberg, P.O., Washenfelder, R.A., Wunch, D., Schneider, T., Toon, G.C., Andres, R.J., Blavier, J.-F., Connor, B., Davis, K.J., Desai, A.R., Messerschmidt, J., Notholt, J., Roehl, C.M., Sherlock, V., Stephens, B.B., Vay, S.A., Wofsy, S.C., 2012. The imprint of surface fluxes and transport on variations in total column carbon dioxide. Biogeosciences 9, 875–891. https://doi.org/10.5194/bg-9-875-2012.
Kim, J., Guo, Q., Baldocchi, D.D., Leclerc, M.Y., Xu, L., Schmid, H.P., 2006. Upscaling fluxes from tower to landscape: overlaying flux footprints on high-resolution (IKONOS) images of vegetation cover. Agric. For. Meteorol. 136, 132–146. https://doi.org/10.1016/j.agrformet.2004.11.015.
Kim, J., Hwang, T., Schaaf, C.L., Kljun, N., Munger, J.W., 2018. Seasonal variation of source contributions to eddy-covariance CO_2 measurements in a mixed hardwood-conifer forest. Agric. For. Meteorol. 253-254, 71–83. https://doi.org/10.1016/j.agrformet.2018.02.004.
Kittler, F., Eugster, W., Foken, T., Heimann, M., Kolle, O., Göckede, M., 2017. High-quality eddy-covariance CO_2 budgets under cold climate conditions. J. Geophys. Res.: Biogeosci. 122, 2064–2084. https://doi.org/10.1002/2017JG003830.
Kljun, N., Rotach, M.W., Schmid, H.P., 2002. A three-dimensional backward Lagrangian footprint model for a wide range of boundary-layer stratifications. Bound. Layer Meteorol. 103, 205–226. https://doi.org/10.1023/A:1014556300021.
Kljun, N., Calanca, P., Rotach, M.W., Schmid, H.P., 2004. A simple parameterization for flux footprint predictions. Bound. Layer Meteorol. 112, 503–523. https://doi.org/10.1023/B:BOUN.0000030653.71031.96.
Kljun, N., Calanca, P., Rotach, M.W., Schmid, H.P., 2015. A simple two-dimensional parameterization for Flux Footprint Prediction (FFP). Geosci. Model Dev. 8, 3695–3713. https://doi.org/10.5194/gmd-8-3695-2015.
Laudon, H., Taberman, I., Ågren, A., Futter, M., Ottosson-Löfvenius, M., Bishop, K., 2013. The Krycklan-Catchment study – a flagship infrastructure for hydrology, biogeochemistry, and climate research in the boreal landscape. Water Resour. Res. 49, 7154–7158. https://doi.org/10.1002/wrcr.20520.
Laudon, H., Hasselquist, E.M., Peichl, M., Lindgren, K., Sponseller, R., Lidman, F., Kuglerová, L., Hasselquist, N.J., Bishop, K., Nilsson, M.B., Ågren, A.M., 2021. Northern landscapes in transition: evidence, approach and ways forward using the Krycklan catchment study. Hydrol. Process 35, e14170. https://doi.org/10.1002/hyp.14170, 2021.
Leclerc, M.Y., Foken, T., 2014. Footprints in Micrometeorology and Ecology. Springer, Berlin, Heidelberg. https://doi.org/10.1007/978-3-642-54545-0.
Martínez-García, E., Nilsson, M.B., Laudon, H., Lundmark, T., Fransson, J.E.S., Wallerman, J., Peichl, M., 2022. Overstory dynamics regulate the spatial variability in forest-floor CO2 fluxes across a managed boreal forest landscape. Agric. For. Meteorol. 318, 108916 https://doi.org/10.1016/j.agrformet.2022.108916.
Mauder, M., Foken, T., 2004. Documentation and Instruction Manual of the Eddy Covariance Software Package TK2. Arbeitsergebnisse Nr. 26. Universität Bayreuth, Abt. Mikrometeorologie, Bayreuth, p. 45.
Mauder, M., Oncley, S.P., Vogt, R., Weidinger, T., Ribeiro, L., Bernhofer, C., Foken, T., Kohsiek, W., De Bruin, H.A.R., Liu, H., 2007. The energy balance experiment EBEX-2000. Part II: intercomparison of eddy-covariance sensors and post-field data processing methods. Bound. Layer Meteorol. 123, 29–54. https://doi.org/10.1007/s10546-006-9139-4.
METEK GmbH, 2012. Turbulence Parameters As Retrieved By uSonic-3 Omni, uSonic-3 Scientific (Former USA-1) and uSonic-3 Class A. METEK GmbH, Germany, p. 19.
Montagnani, L., Grünwald, T., Kowalski, A., Mammarella, I., Merbold, L., Metzger, S., Sedlák, P., Siebicke, L., 2018. Estimating the storage term in eddy covariance measurements: the ICOS methodology. Int. Agrophys. 32, 551–567. https://doi.org/10.1515/intag-2017-0037.
Oren, R., Hsieh, C.I., Stoy, P., Albertson, J., McCarthy, H.R., Harrell, P., Katul, G.G., 2006. Estimating the uncertainty in annual net ecosystem carbon exchange: spatial variation in turbulent fluxes and sampling errors in eddy-covariance measurements. Glob. Chang Biol. 12, 883–896. https://doi.org/10.1111/j.1365-2486.2006.01131.x.
Papale, D., Reichstein, M., Aubinet, M., Canfora, E., Bernhofer, C., Kutsch, W., Longdoz, B., Rambal, S., Valentini, R., Vesala, T., Yakir, D., 2006. Towards a standardized processing of net ecosystem exchange measured with eddy covariance technique: algorithms and uncertainty estimation. Biogeosciences 3, 571–583. https://doi.org/10.5194/bg-3-571-2006.
Peichl, M., ICOS Sweden, 2020a. Ecosystem eco time series (ICOS Sweden), Svartberget, 2017-12-31–2018-12-31, https://hdl.handle.net/11676/TJN0OUllZku0O38SB8N802kG.
Peichl, M., ICOS Sweden, 2020b. Ecosystem eco time series (ICOS Sweden), Svartberget, 2018-12-31–2019-12-31, https://hdl.handle.net/11676/o1EtRqHl-SAoYh1CSvPlgrfK.
Peichl, M., ICOS Sweden, 2020c. Ecosystem meteo time series (ICOS Sweden), Svartberget, 2017-12-31–2018-12-31, https://hdl.handle.net/11676/lUtOVaxHYC9LMtIeG35YURqv.
Peichl, M., ICOS Sweden, 2020d Ecosystem meteo time series (ICOS Sweden), Svartberget, 2018-12-31–2019-12-31, https://hdl.handle.net/11676/89fWI508rv1QHXRj2uhFcqnz.
Peltola, O., Hensen, A., Belelli Marchesini, L., Helfter, C., Bosveld, F.C., van den Bulk, W. C.M., Haapanala, S., van Huissteden, J., Laurila, T., Lindroth, A., Nemitz, E., Röckmann, T., Vermeulen, A.T., Mammarella, I., 2015. Studying the spatial variability of methane flux with five eddy covariance towers of varying height. Agric. For. Meteorol. 214-215, 456–472. https://doi.org/10.1016/j.agrformet.2015.09.007.
Prueger, J.H., Kustas, W.P., 2005. Aerodynamic Methods for Estimating Turbulent Fluxes. American Society of Agronomy, Crop Science Society of America, Soil Science Society of America, Micrometeorology in Agricultural Systems, Agronomy Monograph no. 47, Lincoln, Nebraska, p. 677.
Rannik, Ü., Sogachev, A., Foken, T., Göckede, M., Kljun, N., Leclerc, M.Y., Vesala, T., 2012. Footprint analysis. eds.. In: Aubinet, M., Vesala, T., Papale, D. (Eds.), Eddy Covariance: A Practical Guide to Measurement and Data Analysis. Springer Atmospheric Sciences, Springer, Dordrecht, pp. 211–261. https://doi.org/10.1007/978-94-007-2351-1_8. pages.
Rebmann, C., Kolle, O., Heinesch, B., Queck, R., Ibrom, A., Aubinet, M., 2012. Data acquisition and flux calculations. eds.. In: Aubinet, M., Vesala, T., Papale, D. (Eds.), Eddy Covariance: A Practical Guide to Measurement and Data Analysis. Springer Atmospheric Sciences, Springer, Dordrecht, pp. 59–83. https://doi.org/10.1007/978-94-007-2351-1_3. pages.
Rebmann, C., Aubinet, M., Schmid, H.P., Arriga, N., Aurela, M., Burba, G., Clement, R., De Ligne, A., Fratini, G., Gielen, B., Grace, J., Graf, A., Gross, P., Haapanala, S., Herbst, M., Hörtnagl, L., Ibrom, A., Joly, L., Kljun, N., Kolle, O., Kowalski, A., Lindroth, A., Loustau, D., Mammarella, I., Mauder, M., Merbold, L., Metzger, S., Mölder, M., Montagnani, L., Papale, D., Pavelka, M., Peichl, M., Roland, M., Serrano-Ortiz, P., Siebicke, L., Steinbrecher, R., Tuovinen, J.-P., Vesala, T., Wohlfahrt, G., Franz, D., 2018. ICOS eddy covariance flux-station site setup: a review. Int. Agrophys. 32, 471–494. https://doi.org/10.1515/intag-2017-0044.
Reichstein, M., Falge, E., Baldocchi, D., Papale, D., Aubinet, M., Berbigier, P., Bernhofer, C., Buchmann, N., Gilmanov, T., Granier, A., Grünwald, T., Havránková, K., Ilvesniemi, H., Janous, D., Knohl, A., Laurila, T., Lohila, A., Loustau, D., Matteucci, G., Meyers, T., Miglietta, F., Ourcival, J.-M., Pumpanen, J., Rambal, S., Rotenberg, E., Sanz, M., Tenhunen, J., Seufert, G., Vaccari, F., Vesala, T., Yakir, D., Valentini, R., 2005. On the separation of net ecosystem exchange into assimilation and ecosystem respiration: review and improved algorithm. Glob. Chang. Biol. 11, 1424–1439. https://doi.org/10.1111/j.1365-2486.2005.001002.x.
Ricciuto, D.M., Butler, M.P., Davis, K.J., Cook, B.D., Bakwin, P.S., Andrews, A., Teclaw, R.M., 2008. Causes of interannual variability in ecosystem-atmosphere CO_2 exchange in a norther Wisconsin forest using a Bayesian model calibration. Agric. For. Meteorol. 148, 309–327. https://doi.org/10.1016/j.agrformet.2007.08.007.

Richardson, A.D., Aubinet, M., Barr, A.G., Hollinger, D.Y., Ibrom, A., Lasslop, G., Reichstein, M., 2012. Uncertainty quantification. eds.. In: Aubinet, M., Vesala, T., Papale, D. (Eds.), Eddy Covariance: A Practical Guide to Measurement and Data Analysis. Springer Atmospheric Sciences, Springer, Dordrecht, pp. 173–209. https://doi.org/10.1007/978-94-007-2351-1_7. pages.

Sabbatini, S., Mammarella, I., Arriga, N., Fratini, G., Graf, A., Hörtnagl, L., Ibrom, A., Longdoz, B., Mauder, M., Merbold, L., Metzger, S., Montagnani, L., Pitacco, A., Rebmann, C., Sedlák, P., Šigut, L., Vitale, D., Papale, D., 2018. Eddy covariance raw data processing for CO_2 and energy fluxes calculation at ICOS ecosystem stations. Int. Agrophys. 32, 495–515. https://doi.org/10.1515/intag-2017-0043.

Sathyanadh, A., Monteil, G., Scholze, M., Klosterhalfen, A., Laudon, H., Wu, Z., Gerbig, C., Peters, W., Bastrikov, V., Nilsson, M.B., Peichl, M., 2021. Reconciling the carbon balance of Northern Sweden through integration of observations and modelling. J. Geophys. Res.: Atmosp. 126, e2021JD035185 https://doi.org/10.1029/2021JD035185.

Schmid, H.P., 2002. Footprint modeling for vegetation atmosphere exchange studies: a review and perspective. Agric. For. Meteorol. 113, 159–183. https://doi.org/10.1016/S0168-1923(02)00107-7.

Schmid, H.P., Lloyd, C.R., 1999. Spatial representativeness and the location bias of flux footprints over inhomogeneous areas. Agric. For. Meteorol. 93, 195–209. https://doi.org/10.1016/S0168-1923(98)00119-1.

Schmid, H.P., Su, H.-B., Vogel, C.S., Curtis, P.S., 2003. Ecosystem-atmosphere exchange of carbon dioxide over a mixed hardwood forest in northern lower Michigan. J. Geophys. Res. 108, D14. https://doi.org/10.1029/2002JD003011, 4417.

Schwartz, M.D., Hanes, J.M., Liang, L., 2013. Comparing carbon flux and high-resolution spring phenological measurements in a northern mixed forest. Agric. For. Meteorol. 169, 136–147. https://doi.org/10.1016/j.agrformet.2012.10.014.

Soegaard, H., Jensen, N.O., Boegh, E., Hasager, C.B., Schelde, K., Thomsen, A., 2003. Carbon dioxide exchange over agricultural landscape using eddy correlation and footprint modelling. Agric. For. Meteorol. 114, 153–173. https://doi.org/10.1016/S0168-1923(02)00177-6.

Sogachev, A., Dellwik, E., 2017. Flux footprints for a tall tower in a land-water mosaic area: a case study of the area around the Risø tower. Agric. For. Meteorol. 237-238, 326–339. https://doi.org/10.1016/j.agrformet.2017.02.037.

Vesala, T., Kljun, N., Rannik, Ü., Rinne, J., Sogachev, A., Markkanen, T., Sabelfeld, K., Foken, T., Leclerc, M.Y., 2008. Flux and concentration footprint modelling: state of the art. Environ. Pollut. 152, 653–666. https://doi.org/10.1016/j.envpol.2007.06.070.

Wang, W., Davis, K.J., Cook, B.D., Butler, M.P., Ricciuto, D.M., 2006. Decomposing CO_2 fluxes measured over a mixed ecosystem at a tall tower and extending to a region: a case study. J. Geophys. Res. 111, G02005. https://doi.org/10.1029/2005JG000093.

Webster, R., 1997. Regression and functional relations. Eur. J. Soil Sci. 48, 557–566. https://doi.org/10.1111/j.1365-2389.1997.tb00222.x.

Wharton, S., Schroeder, M., Paw, U., KT, Falk, M., Bible, K., 2009. Turbulence considerations for comparing ecosystem exchange over old-growth and clear-cut stands for limited fetch and complex canopy flow conditions. Agric. For. Meteorol. 149, 1477–1490. https://doi.org/10.1016/j.agrformet.2009.04.002.

Wutzler, T., Lucas-Moffat, A., Migliavacca, M., Knauer, J., Sickel, K., Šigut, L., Menzer, O., Reichstein, M., 2018. Basic and extensible post-processing of eddy covariance data with REddyProc. Biogeosciences 15, 5015–5030. https://doi.org/10.5194/bg-15-5015-2018.

Xu, K., Metzger, S., Desai, A.R., 2017. Upscaling tower-observed turbulent exchange at fine spatio-temporal resolution using environmental response functions. Agric. For. Meteorol. 232, 10–22. https://doi.org/10.1016/j.agrformet.2016.07.019.

Zhang, X., Lee, X., Griffis, T.J., Baker, J.M., Xiao, W., 2014. Estimating regional greenhouse gas fluxes: an uncertainty analysis of planetary boundary layer techniques and bottom-up inventories. Atmosp. Chem. Phys. 14, 10705–10719. https://doi.org/10.5194/acp-14-10705-2014.